

# Dressed state approach to matter wave mixing of bosons

E. Rowen, R. Ozeri, N. Katz, R. Pugatch, and N. Davidson

*Department of Physics of Complex Systems,  
Weizmann Institute of Science, Rehovot 76100, Israel*

(Dated: March 23, 2022)

## Abstract

A dressed state approach to mixing of bosonic matter waves is presented. Two cases are studied using this formalism. In the first, two macroscopically populated modes of atoms (two-wave mixing) are coupled through the presence of light. In the second case, three modes of Bogoliubov quasiparticles (three-wave mixing) are coupled through s-wave interaction. In both cases wave mixing induces oscillations in the population of the different modes that decay due to interactions. Analytic expressions for the dressed basis spectrum and the evolution of the mode populations in time are derived both for resonant mixing and non-resonant mixing. Oscillations in the population of a given mode are shown to lead to a splitting in the decay spectrum of that mode, in analogy to the optical Autler-Townes splitting in the decay spectrum of a strongly driven atom. These effects cannot be described by a mean-field approximation.

PACS numbers: 03.75.Gg

## I. INTRODUCTION

Wave mixing is a well known phenomenon which occurs in nonlinear systems. The realization of Bose-Einstein condensates (BEC) in atomic vapor paved the path to the experimental study of mixing of matter waves [1, 2, 3], in which the s-wave interactions are the cause for the required nonlinearity. This exciting new effect is analogous to the wave mixing of optical modes in nonlinear processes such as parametric down-conversion [4]. As in the optical case, atomic wave mixing is predicted to generate number squeezed states. These states are usually referred to as quantum states with a well defined number and a spread in the phase, contrary to the BEC itself, which is described well by a classical wave in the sense that both number and phase are well defined. These squeezed states can be used to perform sub-shotnoise measurements in interferometry experiments [5].

In previous work, the nonlinear mixing of Bogoliubov quasiparticles was studied using the Gross-Pitaevskii equation (GPE) [6]. In the high momentum limit, in which most experiments are performed, atomic four-wave mixing was studied using the GPE [7], and analyzed directly in the quantum many body formalism using angular momentum for mixing of different hyperfine modes [8]. The coherence in wave mixing of two light modes with two atomic modes was studied experimentally [9] and demonstrated when only one atomic mode and one light mode are initially populated [10, 11].

Many dynamical effects in ultra-cold atoms can be described by the time dependent GPE, which governs the evolution of a macroscopically occupied wavefunction. This approach cannot be used in order to study quantum effects where number and phase cannot both be determined at once. Here we develop a dressed state model [12], which unlike the GPE, does *not* assume all atoms are in the same single particle state. We use this model to describe effects that are beyond mean-field, such as dephasing due to quantum uncertainty in Rabi oscillations between momentum modes, and the decay of a matter wave due to interaction with the quasi-continuum of unoccupied modes.

Weak interactions are usually taken into account by the Bogoliubov transformation from the atomic basis to a basis of quasiparticles. Interactions between quasiparticles and their decay were first analyzed by Beliaev [13], and experimentally verified [14, 15]. In this paper we study wave mixing between macroscopically occupied quasiparticle modes. For simplicity we consider throughout the paper only homogeneous condensates at  $T = 0$ . We find that

interactions between quasiparticles can lead to new phenomena in matter waves, analogous to phenomena studied in connection to interactions of light waves with matter, such as a splitting in the decay spectrum, power broadening and energy shifts [16]. We first apply the dressed state formalism to the simple case of two matter waves coupled by laser fields. We then adapt it to solve the more interesting case of three-wave mixing as a locally perturbed two-wave mixing.

Treating the wave mixing problem in the Bogoliubov basis allows us to consider mixing between quasiparticles in the low momentum regime, where the basis of atomic modes (used e.g. to describe four-wave mixing of matter waves [1, 3]) is not appropriate due to the large  $-\mathbf{k}$  atomic component of a quasiparticle with momentum  $\mathbf{k}$ . Such a low momentum regime is of particular interest since both the density of states and quantum interference effects yield very low decay rates [15, 17], and is therefore more suitable experimentally for the study of relative number squeezing and entanglement between matter waves. In the high momentum regime, three-wave mixing coincides with the conventional four-wave mixing of matter waves as long as the condensate, which is the fourth wave, is not substantially depleted.

The layout of this paper is as follows: First, in section II we review the Bogoliubov transformation and the wave mixing Hamiltonians for two physical scenarios. We describe both the mixing of Bogoliubov quasiparticles due to the s-wave interaction, and the mixing of atomic modes which are coupled by laser fields, and in which case interactions may be included as a perturbation. We also derive the perturbative dynamics and energy shifts due to the interactions between Bogoliubov quasiparticles. Next, in section III, we solve the two-wave mixing Hamiltonian. For noninteracting atoms, this is in fact a single particle problem. However, we use the second-quantized formalism, which will become a necessity once interactions are introduced, and nonlinear dynamics emerge. We compare this formalism to the two-mode Gross Pitaevskii model [18], and discuss the dynamical instability, as well as a decay due to quantum uncertainty in the number of quasiparticles. In section IV we turn to the nonlinear three-wave mixing between Bogoliubov quasiparticles, using the framework introduced in section III. We study the dynamics and spectrum of resonant and non-resonant three-wave mixing. We find an analytic approximation which is in good agreement with numerical diagonalization, and derive the scaling laws which let us describe a realistic system by matrices which can be diagonalized on a personal computer. Finally, in section V, we discuss the decay of a quasiparticle coupled both to a quasi-continuum and

an additional macroscopically occupied quasiparticle mode. We find a splitting in the decay spectrum in analogy to the Autler-Townes splitting of the spectrum of an atom undergoing Rabi oscillations. We conclude with a brief summary and examples of other cases to which our formalism can be applied.

## II. WAVE MIXING HAMILTONIANS FOR ULTRA-COLD ATOMS

In this paper we concentrate on a homogeneous system of ultra-cold bosons, with s-wave interactions. We use this system to derive the physical Hamiltonians giving rise to two and three-wave mixing. The three-wave mixing is of Bogoliubov quasiparticles over a condensate which are inherently coupled by interactions. It therefore describes interactions correctly even for small momentum modes, but is not applicable to strong excitations which deplete the condensate [19]. The two-wave mixing is of two macroscopically populated momentum modes, which can be depleted, and are coupled by an external laser field. Interactions are incorporated as a mean-field shift, thus the two-wave model is not applicable for small momenta.

### A. Wave mixing of Bogoliubov quasiparticles

In momentum representation the Hamiltonian governing a system of ultra-cold interacting bosons is given by [20]:

$$H = \sum_{\mathbf{k}} \frac{\hbar^2 k^2}{2M} \hat{a}_{\mathbf{k}}^\dagger \hat{a}_{\mathbf{k}} + \frac{g}{2V} \sum_{\mathbf{k}, \mathbf{l}, \mathbf{m}} \hat{a}_{\mathbf{k}}^\dagger \hat{a}_{\mathbf{l}}^\dagger \hat{a}_{\mathbf{m}} \hat{a}_{\mathbf{k}+\mathbf{l}-\mathbf{m}}. \quad (1)$$

$g = 4\pi\hbar^2 a_s / M$  is a constant proportional to the scattering length  $a_s$ , describing the atom-atom interaction.  $V$  is the volume of the condensate and  $M$  is the atomic mass. Assuming a macroscopic occupation of the ground state  $N_0$ , thus replacing both  $\hat{a}_0$  and  $\hat{a}_0^\dagger$  by  $\sqrt{N_0}$  this Hamiltonian is diagonalized to quadratic order by the Bogoliubov transformation

$$\hat{a}_{\mathbf{k}} = u_k \hat{b}_{\mathbf{k}} - v_k \hat{b}_{-\mathbf{k}}^\dagger \quad (2)$$

$$\hat{a}_{\mathbf{k}}^\dagger = u_k \hat{b}_{\mathbf{k}}^\dagger - v_k \hat{b}_{-\mathbf{k}}. \quad (3)$$

When taken to cubic terms in  $\hat{b}$ , Eq. (1) can be written as  $H = H_0 + H_{int}$  with

$$H_0 = E_g + \sum_{\mathbf{k}'} \epsilon_{\mathbf{k}'} \hat{b}_{\mathbf{k}'}^\dagger \hat{b}_{\mathbf{k}'}, \quad (4)$$

where  $E_g$  is the energy of the Bogoliubov vacuum, and

$$H_{int} = \frac{g\sqrt{N_0}}{2V} \sum_{\mathbf{k}', \mathbf{q}'} \left[ A_{\mathbf{k}', \mathbf{q}'} \left( \hat{b}_{\mathbf{k}'} \hat{b}_{\mathbf{q}'}^\dagger \hat{b}_{\mathbf{k}' - \mathbf{q}'}^\dagger + \hat{b}_{\mathbf{k}'}^\dagger \hat{b}_{\mathbf{q}'} \hat{b}_{\mathbf{k}' - \mathbf{q}'} \right) + B_{\mathbf{k}', \mathbf{q}'} \left( \hat{b}_{\mathbf{k}'}^\dagger \hat{b}_{\mathbf{q}'}^\dagger \hat{b}_{-(\mathbf{k}' + \mathbf{q}')}^\dagger + \hat{b}_{\mathbf{k}'} \hat{b}_{\mathbf{q}'} \hat{b}_{-(\mathbf{k}' + \mathbf{q}')} \right) \right]. \quad (5)$$

For weakly excited condensates  $H_{int}$  is typically small, and is usually neglected, as in the derivation of the Bogoliubov spectrum  $\epsilon_k = \sqrt{\frac{\hbar^2 k^2}{2M} \left( \frac{\hbar^2 k^2}{2M} + 2\mu \right)}$ , where  $\mu = g\rho$  is the chemical potential and  $\rho$  is the condensate density. The quasiparticle modes which diagonalize  $H_0$  interact via  $H_{int}$ . The terms  $A_{\mathbf{k}, \mathbf{q}}$ ,  $B_{\mathbf{k}, \mathbf{q}}$  are combinations of the  $u$ 's and  $v$ 's originating from interference between different atomic collision pathways, and are given by

$$A_{\mathbf{k}, \mathbf{q}} = 2u_k (u_q u_{|\mathbf{k} - \mathbf{q}|} - u_q v_{|\mathbf{k} - \mathbf{q}|} - v_q u_{|\mathbf{k} - \mathbf{q}|}) - 2v_k (v_q v_{|\mathbf{k} - \mathbf{q}|} - v_q u_{|\mathbf{k} - \mathbf{q}|} - u_q v_{|\mathbf{k} - \mathbf{q}|}) \quad (6)$$

$$B_{\mathbf{k}, \mathbf{q}} = 2u_k (v_q v_{|\mathbf{k} - \mathbf{q}|} - u_q v_{|\mathbf{k} - \mathbf{q}|} - v_q u_{|\mathbf{k} - \mathbf{q}|}) - 2v_k (u_q u_{|\mathbf{k} - \mathbf{q}|} - v_q u_{|\mathbf{k} - \mathbf{q}|} - u_q v_{|\mathbf{k} - \mathbf{q}|}). \quad (7)$$

$A_{\mathbf{k}, \mathbf{q}}$  and  $B_{\mathbf{k}, \mathbf{q}}$  are symmetric under the exchange  $\mathbf{q} \leftrightarrow \mathbf{k} - \mathbf{q}$ , as implied by Eq. (5). The different terms of  $H_{int}$  describe different processes resulting from the quasiparticle interactions. These processes are described diagrammatically in Fig. 1. The first term in Eq. (5) corresponds to the decay of one quasiparticle into two, and is analogous to parametric down conversion. This decay is referred to as Beliaev damping. The second term describes two quasiparticles colliding, and forming one quasiparticle with the total momentum. This term governs the so called Landau damping. The last two terms in  $H_{int}$  (proportional to  $B_{\mathbf{k}', \mathbf{q}'}$ ) describe the spontaneous formation and annihilation of three quasiparticles with zero total momentum.

### 1. Resonant wave mixing

Consider the case where there are initially  $N \ll N_0$  excitations in the momentum mode  $\mathbf{k}$ , and no other excitations. The state  $|N_{\mathbf{k}}\rangle$  is degenerate under  $H_0$  with the states  $|(N-1)_{\mathbf{k}}, 1_{\mathbf{q}'}, 1_{\mathbf{k}-\mathbf{q}'}\rangle$  for those  $\mathbf{q}'$  that fulfill the resonance condition

$$\epsilon_{\mathbf{q}'} + \epsilon_{|\mathbf{k}-\mathbf{q}'|} = \epsilon_{\mathbf{k}}. \quad (8)$$

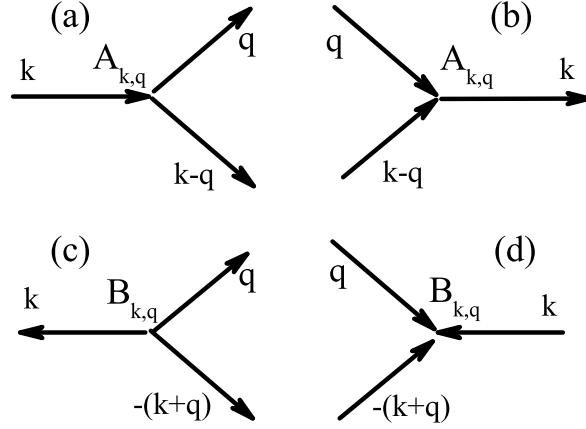


FIG. 1: The four processes described by  $H_{int}$  in Eq. (5): (a) Beliaev damping (b) Landau damping (c) spontaneous creation of 3 quasiparticles (d) spontaneous annihilation of 3 quasiparticles. Only processes (a) and (b) can be resonant.

The mode  $\mathbf{k}$  can therefore decay via the Beliaev term in  $H_{int}$  into pairs of modes on a shell of a quasi-continuum of modes conserving both energy and momentum. The decay rate  $\Gamma$  is approximated by the Fermi golden rule (FGR) [12]:

$$\Gamma = \frac{2\pi}{\hbar} \frac{g^2 N_0 N}{4V^2} \frac{1}{2} \sum_{\mathbf{q}'} |2A_{\mathbf{k},\mathbf{q}'}|^2 \delta(\epsilon_{\mathbf{k}} - \epsilon_{\mathbf{q}'} - \epsilon_{\mathbf{k}-\mathbf{q}'}). \quad (9)$$

The factors of 2 in Eq. (9) are due to bosonic exchange symmetry between  $\mathbf{q}'$  and  $\mathbf{k} - \mathbf{q}'$ . The FGR is valid as long as the quasi-continuum contains enough modes  $N_c$  such that during the time of the experiment the average population of these modes will be less than 1, i.e.  $\Gamma t \ll N_c$ . The second (Landau) term in  $H_{int}$  does not contribute to the evolution at temperatures much lower than the chemical potential, since there is only a negligible occupation of modes other than  $\mathbf{k}$ . The third and forth terms have no contribution to the decay since they do not conserve energy.

Now consider the evolution of the same state  $|N_{\mathbf{k}}\rangle$ , when there is an initial seed of  $M$  excitations of mode  $\mathbf{q}$  which satisfies the resonance condition [Eq.(8)], i.e. it is on the energy-momentum conserving shell. Our initial condition is thus  $|(N)_{\mathbf{k}}, (M)_{\mathbf{q}}\rangle$ . Such a situation is presented schematically in momentum space in Fig. 2a. The condensate, which is the quasiparticle vacuum is represented by a dark gray ellipse. The initially occupied quasiparticle modes are plotted as light gray ellipses, and the initially unpopulated mode

$\mathbf{k} - \mathbf{q}$  is represented as an empty ellipse. The line describes the quasi-continuum of possible modes for Beliaev damping from mode  $\mathbf{k}$ . For  $M \ll N_c$  the initially occupied mode  $\mathbf{q}$  will merely enhance the decay rate in Eq. (9) to

$$\Gamma_M = \Gamma + \frac{2\pi M}{2\hbar} \frac{g^2 N_0 N A_{\mathbf{k},\mathbf{q}}}{V^2}. \quad (10)$$

This enhancement of  $\Gamma$  is analogous to the optical power-broadening, where an occupied mode of the electromagnetic field broadens the natural linewidth of an atom  $\Gamma$ , which is also the decay rate due to spontaneous emission [16]. If, however  $M > N_c$ , a situation that is experimentally achievable in cold atoms where  $N_c \sim 10^3 - 10^4$ , the dynamics are changed significantly from the simple decay. The term containing  $\mathbf{k}, \mathbf{q}$  in the sum will dominate  $H_{int}$  in Eq. (5) and decay into two unpopulated modes can be neglected, yielding  $H_{int} \approx H_{3W}^{res}$ , where we define the resonant three-wave Hamiltonian as

$$H_{3W}^{res} = \frac{g\sqrt{N_0}}{2V} \left[ A_{\mathbf{k},\mathbf{q}} \left( \hat{b}_{\mathbf{k}}^\dagger \hat{b}_{\mathbf{k}-\mathbf{q}} \hat{b}_{\mathbf{q}} + \hat{b}_{\mathbf{k}} \hat{b}_{\mathbf{k}-\mathbf{q}}^\dagger \hat{b}_{\mathbf{q}}^\dagger \right) \right]. \quad (11)$$

Since the modes  $\mathbf{q}$  and  $\mathbf{k} - \mathbf{q}$  will both become macroscopically occupied, the second term in Eq. (11) cannot be ignored. This case will be studied in section IV. Since the states  $|(N - n)_{\mathbf{k}}, (M + n)_{\mathbf{q}}, n_{\mathbf{k}-\mathbf{q}}\rangle$  with different  $n$  are degenerate under  $H_0$ , the eigenstates of  $H_{3W}^{res}$  in this subspace are also eigenstates of  $H$ , and once calculated, both dynamics and spectra are extracted in a straightforward manner. In sections IV and V  $H_{3W}^{res}$  will lead to nonlinear oscillations, and a splitting in the decay spectrum of the mode  $\mathbf{k}$ .

## 2. Non-resonant wave mixing

The non-resonant terms of  $H_{int}$  in Eq. (5) do not contribute to the perturbative dynamics. They do, however, lead to energy shifts. Using second order perturbation theory we find an energy shift of the Bogoliubov quasiparticle energy of mode  $\mathbf{k}$  by

$$\delta\epsilon_k = \frac{g^2 N_0}{4V^2} \wp \sum_{\mathbf{q}'} \left[ \frac{|2A_{\mathbf{k},\mathbf{q}'}|^2}{2(\epsilon_k - \epsilon'_q - \epsilon_{|\mathbf{k}-\mathbf{q}|})} - \left( \frac{|6B_{\mathbf{k},\mathbf{q}'}|^2}{2(\epsilon_k + \epsilon'_q + \epsilon_{|\mathbf{k}+\mathbf{q}|})} \right) \right], \quad (12)$$

where  $\wp$  stands for the principal part. This energy shift is analogous to the Lamb shift of atomic states due to the Electromagnetic vacuum [16]. In analogy to the resonant wave mixing, we study the Hamiltonian (5), again with the initial condition  $|(N)_{\mathbf{k}}, (M)_{\mathbf{q}}\rangle$ . This time we consider the case where the mode  $\mathbf{q}$  is not on the energy-momentum conserving

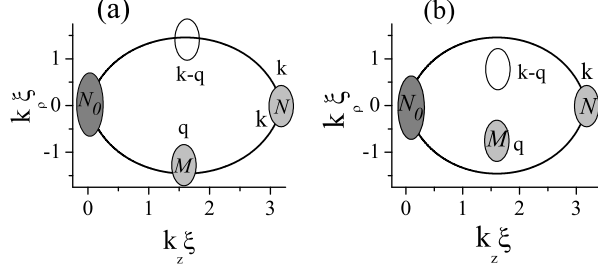


FIG. 2: A schematic momentum-space description of three-wave mixing. (a) The  $M$ -fold occupation of the seed mode  $\mathbf{q}$  fulfills the resonance condition of Eq. (8), and is therefore on the solid line which marks the quasi-continuum of possible states for Beliaev damping of mode  $\mathbf{k}$ . (b) The seed mode  $\mathbf{q}$  is *not* on the energy conserving shell, leading to non-resonant wave mixing. In both figures the condensate is marked as a dark gray ellipse, the initially occupied modes are marked as light gray ellipses, and the empty modes which fulfill momentum conservation are represented as empty ellipses. The shell of possible modes is calculated for  $k\xi = 3.2$ , and is therefore not completely spherical as expected for atomic s-wave scattering, but rather lemon-shaped [15]. Note that only in the high momentum limit do the plotted modes correspond to atomic momentum modes.

shell defined by Eq. (8), but is rather detuned by  $\hbar\Delta = \epsilon_{\mathbf{q}} + \epsilon_{|\mathbf{k}-\mathbf{q}|} - \epsilon_{\mathbf{k}}$ , as schematically shown in Fig. 2b. We consider small values of detuning  $\hbar\Delta \ll \epsilon_k, \epsilon_q$ , hence we neglect the terms  $B_{\mathbf{k},\mathbf{q}}$  in Eq. (5) since the energy denominators of the  $B_{\mathbf{k},\mathbf{q}}$  terms are much larger than those of the  $A_{\mathbf{k},\mathbf{q}}$  terms. This is in analogy to the rotating wave approximation in optics. To keep the states  $|(N-n)_{\mathbf{k}}, n_{\mathbf{k}-\mathbf{q}}, (M+n)_{\mathbf{q}}\rangle$  degenerate under  $H_0$ , Eq. (4) is modified to the form  $H_0 = E_g + \sum_{\mathbf{k}'} \epsilon_{k'} \hat{b}_{\mathbf{k}'}^\dagger \hat{b}_{\mathbf{k}'} - \hat{b}_{|\mathbf{k}-\mathbf{q}|}^\dagger \hat{b}_{|\mathbf{k}-\mathbf{q}|} \Delta$ . In order for  $H$  to remain the same as in Eq. (5) we must generalize  $H_{3W}^{res}$  to

$$H_{3W} = \frac{g\sqrt{N_0}}{2V} \left[ A_{\mathbf{k},\mathbf{q}} \left( \hat{b}_{\mathbf{k}}^\dagger \hat{b}_{\mathbf{q}} \hat{b}_{\mathbf{k}-\mathbf{q}} + \hat{b}_{\mathbf{k}} \hat{b}_{\mathbf{q}}^\dagger \hat{b}_{\mathbf{k}-\mathbf{q}}^\dagger \right) \right] + \hat{b}_{|\mathbf{k}-\mathbf{q}|}^\dagger \hat{b}_{|\mathbf{k}-\mathbf{q}|} \Delta. \quad (13)$$

We will show in section V that  $H_{int}$  leads to a splitting in the damping spectrum of mode  $\mathbf{k}$ . The detuning leads to an asymmetry in the peaks. When the detuning is large (but still smaller than  $\epsilon_k/\hbar$ ), one peak vanishes, and the other peak dominates. The large peak is shifted from  $\epsilon_k$  due to the macroscopically occupied mode  $\mathbf{q}$  by

$$\delta\epsilon_k = -\frac{g^2 N_0 M}{V^2} \frac{|A_{\mathbf{k},\mathbf{q}}|^2}{2\Delta}. \quad (14)$$

This shift in the spectrum is analogous to the ac-Stark shift and appears in addition to the Lamb shift of Eq. (12).



## B. Wave mixing due to Bragg coupling

The interaction Hamiltonian described in Eq. (5) takes into account the quantum depletion of atoms from the  $\mathbf{k} = 0$  mode in the many-body ground state of the BEC due to interactions. In fact, this effect is what leads to the momentum dependence of  $A_{\mathbf{k},\mathbf{q}}$ . However Eq. (5) is derived under the assumption that at all times the population in all modes much is smaller than  $N_0$ , i.e. the condensate is undepleted. There are cases where the condensate is depleted, for example by a strong two-photon Bragg coupling leading to Rabi oscillations between momentum modes 0 and  $\mathbf{k}_B$  [19]. The Bragg coupling is characterized by a frequency  $\omega_B$  and a wavevector  $\mathbf{k}_B$ , that are the difference in the laser frequencies and wavevectors respectively and by an effective Rabi frequency  $\Omega$  which describes the coupling strength. The detuning of the Bragg pulse is  $\delta = \omega_B - \hbar k_B^2/2M$ . In the rotating wave approximation ( $\delta \ll \hbar k_B^2/2M$ ) the resonant Bragg pulse couples the macroscopically occupied mode  $\mathbf{k} = 0$  to  $\mathbf{k}_B$ , so we may estimate the effect of the Bragg pulse as [21]:

$$H_{2W}^{res} = \frac{\hbar\Omega}{2} \left( \hat{a}_0^\dagger \hat{a}_{\mathbf{k}_B} + \hat{a}_0 \hat{a}_{\mathbf{k}_B}^\dagger \right), \quad (15)$$

where we have neglected coupling to all other momentum modes  $(-\mathbf{k}_B, 2\mathbf{k}_B, \dots)$  which are far off resonance. So far interactions are not included in this subsection, and therefore we use the atomic basis rather than a quasiparticle basis. As in Eq. (13), for a detuning from resonance that is much smaller than the detuning from other momentum modes ( $|\delta| \ll |\omega_B - \hbar(mk_B)^2/2M|$  for  $m \neq 1$ ), the Bragg Hamiltonian is simply modified to

$$H_{2W} = \frac{\hbar\Omega}{2} \left( \hat{a}_0^\dagger \hat{a}_{\mathbf{k}_B} + \hat{a}_0 \hat{a}_{\mathbf{k}_B}^\dagger \right) - \hbar\delta \hat{n}_{\mathbf{k}_B}. \quad (16)$$

Here  $\hat{n}_{\mathbf{k}} = \hat{a}_{\mathbf{k}}^\dagger \hat{a}_{\mathbf{k}}$  is the number operator of mode  $\mathbf{k}$ . Neglecting interactions between the atoms,  $H_{2W}$  describes the single particle two level system. If one adds  $H_{2W}$  to the Hamiltonian (1), it is no longer possible to use the Bogoliubov approximation, since the Bragg process depletes the condensate. One can however include atomic interactions by taking only the  $\mathbf{k} = 0$  and the  $\mathbf{k} = \mathbf{k}_B$  modes into account in the interaction term in Eq. (1). This amounts to neglecting terms proportional to  $v_k^2$  in the Hamiltonian, such as the quantum depletion of the condensate. Neglecting  $v_k$  and approximating  $u_k \approx 1$  is a good approximation for momenta larger than the inverse of the healing length  $\xi = (8\pi\rho a_s)^{-1/2}$ . In this regime the Bogoliubov quasiparticle energy is a free particle parabola shifted by the mean-field energy

$\mu$ , and the quasiparticle wavefunction is equal to the free particle wavefunction [20]. The coupling Hamiltonian including the resonant Bragg coupling and the atomic interactions of momentum modes 0 and  $\mathbf{k}_B$  can be written as:

$$H_{2W}^{int} = \frac{\hbar\Omega}{2} \left( \hat{a}_0^\dagger \hat{a}_{\mathbf{k}_B} + \hat{a}_0 \hat{a}_{\mathbf{k}_B}^\dagger \right) + \frac{g}{2V} [\hat{n}_0 (\hat{n}_0 - 1) + \hat{n}_{\mathbf{k}_B} (\hat{n}_{\mathbf{k}_B} - 1) + 4\hat{n}_0 \hat{n}_{\mathbf{k}_B}]. \quad (17)$$

Using the conservation of particles  $\hat{n}_0 + \hat{n}_{\mathbf{k}_B} = N$ , the interaction term in Eq. (17) can be simplified to  $(N^2 - N + 2\hat{n}_0 \hat{n}_{\mathbf{k}_B})g/2V$ . For a small excitation, i.e.  $n_{\mathbf{k}_B} \ll n_0$ , this coincides with the mean-field energy  $\hat{n}_{\mathbf{k}_B} \mu$  of Bogoliubov quasiparticles, while for a nearly depleted condensate, where  $n_0 \ll n_{\mathbf{k}_B}$ , the energy is the same due to the symmetry  $n_0 \leftrightarrow n_{\mathbf{k}_B}$ . This situation describes a condensate that is moving in the lab frame of reference with momentum  $\mathbf{k}_B$  and  $n_0$  excitations with momentum  $-\mathbf{k}_B$  relative to the condensate. Here the mean field energy per quasiparticle is  $gn_{\mathbf{k}_B}/V$ .  $H_{2W}^{int}$  is no longer a linear Hamiltonian and cannot be solved in first quantization as a single particle problem. In fact, even the Gross-Pitaevskii equation is inadequate for solving this Hamiltonian for certain parameters [18]. The Hamiltonians (15-17) are studied in section III. Systems governed by Eq. (17) also exhibit oscillations, a splitting in the excitation spectrum and a variation in the decay spectrum. These phenomena have been demonstrated experimentally [19, 22].

### III. TWO-WAVE MIXING

In this section we discuss the diagonalization of the two-wave mixing Hamiltonians (15-17). We start with Eq. (15). Although this is a single atom problem (since it includes no interactions) we diagonalize the Hamiltonian in second quantization, in order to develop a notation used later for problems such as three-wave mixing which are many-body in nature. In subsection IIIC we use this simple notation to describe the perturbative dynamics of a many-body problem including s-wave interactions between the atoms oscillating between large momentum modes.

Although  $H_{2W}$  involves two fields, the conserved quantity  $N = \hat{a}_0^\dagger \hat{a}_0 + \hat{a}_{\mathbf{k}_B}^\dagger \hat{a}_{\mathbf{k}_B}$  allows us to diagonalize in a subspace with one quantum number  $n = n_{\mathbf{k}_B}$ , varying between 0 and  $N$ , and representing a Fock state  $|n\rangle = |(N - n)_0, n_{\mathbf{k}_B}\rangle$ .

$H_{2W}$  couples between states in this subspace which have a difference of 1 in the quantum number  $n$ , and can be represented in the resonant case by the  $(N + 1) \times (N + 1)$  tri-diagonal

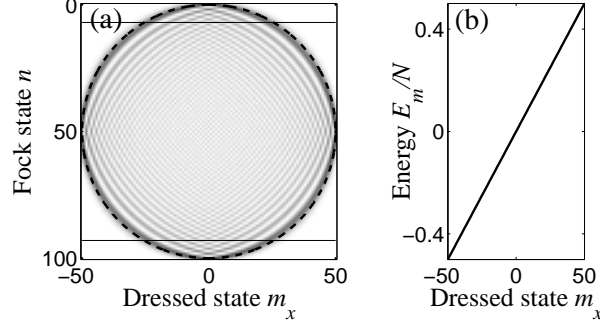


FIG. 3: (a) Absolute value squared of the transformation matrix between the Fock basis and the dressed basis which diagonalizes  $H_{2W}^{res}$  given in Eq. (15)  $|\langle n|m_x \rangle|^2$ , for  $N = 100$ . Dashed line is the circle  $(n - j)^2 + m_x^2 = j^2$ . The thin horizontal lines show the location of the  $n = 7$  and  $n = N - 7$  rows which are plotted in Fig. 4. (b) The spectrum of  $H_{2W}^{res}$ , which is strictly linear. Energy is in units of  $\hbar\Omega$

matrix

$$H_{2W}^{res} = \frac{\hbar\Omega}{2} \begin{pmatrix} 0 & \sqrt{1(N-0)} & 0 & \cdots & \\ \sqrt{1(N-0)} & 0 & \sqrt{2(N-1)} & & \\ 0 & \sqrt{2(N-1)} & 0 & \ddots & \\ \vdots & & \ddots & \ddots & \sqrt{(N-0)1} \\ & & & \sqrt{(N-0)1} & 0 \end{pmatrix} \quad (18)$$

When  $H_{2W}^{res}$  is diagonalized, we get a new set of  $N + 1$  eigenstates, that are dressed by the interaction, labelled by the quantum numbers  $m_x$ , which can take  $N + 1$  different values.

The squared absolute value of the matrix elements of the transformation matrix between the Fock states  $|n\rangle$  and the dressed states  $m_x$ , are shown in Fig. 3 for  $N = 100$ , along with the corresponding eigen-energies. As can be seen, the spectrum is linear,  $E_{m_x} = \hbar\Omega N m_x$ , indicating this is indeed a single particle problem. Once the transformation matrix is solved, dynamics can be calculated trivially by projecting the initial state on the dressed basis and evolving each dressed state according to  $|m_x(t)\rangle = e^{-iE_{m_x}t/\hbar} |m_x(0)\rangle$ , yielding the well known Rabi oscillations, with frequency  $\Omega$ . These oscillations have been demonstrated experimentally [23].

### A. The Schwinger boson mapping

We now turn to describing the problem in terms of angular momentum. For non-interacting resonant coupling the exact solution was found by Tavis and Cummings [24]. This approach will prove to be useful later when we deal with problems which are no longer linear. The two dimensional harmonic oscillator can be solved in different bases. Each oscillator can be solved separately and the eigenfunctions are tensor products of one dimensional oscillators. Another option is to work in polar coordinates, and find eigenstates of angular momentum and of the radial equation. The Schwinger boson mapping [25, 26] maps the Fock basis of decoupled one dimensional harmonic oscillators, with a fixed sum of excitations  $N = n_0 + n_{\mathbf{k}_B}$  onto the angular momentum basis with a fixed total angular momentum  $j = N/2$ . The mapping is defined by the following operators

$$\hat{J}^+ \equiv \hat{a}_0 \hat{a}_{\mathbf{k}_B}^\dagger, \quad (19)$$

$$\hat{J}^- \equiv \hat{a}_{\mathbf{k}_B} \hat{a}_0^\dagger, \quad (20)$$

$$\hat{J}_z \equiv \frac{1}{2} \left( \hat{a}_{\mathbf{k}_B}^\dagger \hat{a}_{\mathbf{k}_B} - \hat{a}_0^\dagger \hat{a}_0 \right). \quad (21)$$

Both representations fulfill the angular momentum commutation relations, and this mapping is completed by associating the quantum numbers

$$m_z \equiv \frac{n_{\mathbf{k}_B} - n_0}{2}, \quad (22)$$

$$j \equiv \frac{n_{\mathbf{k}_B} + n_0}{2} = \frac{N}{2}. \quad (23)$$

Thus a state  $|(N - n)_0, n_{\mathbf{k}_B}\rangle$  in the Fock basis is equivalent to the state  $|j = N/2, m_z = n_{\mathbf{k}_B} - N/2\rangle$  in the angular momentum basis. Using this mapping we write the Hamiltonian in the angular momentum basis simply as

$$H_{2W}^{res} = \frac{1}{2} \hbar \Omega (\hat{J}^+ + \hat{J}^-) = \hbar \Omega \hat{J}_x. \quad (24)$$

The eigenstates of  $H_{2W}^{res}$ , which we refer to as dressed states, are labelled by their projection on the  $x$  axis  $m_x = -j, \dots, j$ , rather than their projection on the  $z$  axis  $m_z = n - j$ , and the spectrum is linear  $E_{m_x} = \hbar \Omega m_x$ . The transformation matrix from the Fock basis to the dressed basis, shown in Fig. 3, is also straightforward to understand in this representation, and is simply a  $N+1$  dimensional representation of an  $SO(3)$  rotation around the  $y$  axis by an

angle  $\theta = -\pi/2$  with matrix elements, known as the Wigner matrix elements,  $d_{m_x, m_z}^j(-\pi/2)$ , which are defined analytically in [27].

In the limit of large  $j$ , we can use classical reasoning to predict the shape of the transformation matrix. A classical spin of length  $j$  with a projection  $m_z$  on the  $z$  axis could be found anywhere on a circle of radius  $\sqrt{j^2 - m_z^2}$  in the  $x$ - $y$  plane with equal probability. Therefore, the probability to measure a certain projection  $m_x$  on the  $x$  axis vanishes for  $|m_x| > \sqrt{j^2 - m_z^2}$  and is proportional to  $(j^2 - m_z^2)^{-1/2}$  for  $|m_x| < \sqrt{j^2 - m_z^2}$ . For this reason we expect that for large enough representations, the transformation matrix should be bounded by the circle  $m_x^2 + m_z^2 = j^2$ , and its amplitude should peak on this circle. In Fig. 3(a), this circle is plotted as a dashed line. Indeed, the largest amplitudes are found on this circle, and the amplitudes outside are completely negligible.

$H_{2W}^{res}$  is analogous to the Hamiltonian of a magnetic field in the  $X$  direction applied to a spin  $j$  particle. The spectrum presented in Fig. 3(b) is therefore analogous to the Zeeman energy of that particle.

If one of the momentum modes, say 0, has a large occupation, the operator  $\hat{a}_0^\dagger \hat{a}_{\mathbf{k}_B} + \hat{a}_{\mathbf{k}_B}^\dagger \hat{a}_0$  can be estimated by  $\sqrt{n_0}(\hat{a}_{\mathbf{k}_B}^\dagger + \hat{a}_{\mathbf{k}_B})$  which is proportional to the position operator for the mode  $\mathbf{k}_B$ , whose eigenfunctions are the single harmonic oscillator wavefunctions. Therefore for  $n$  close enough to 0 the representation of the Fock states in the dressed basis are indeed very similar to the eigenfunctions of a single harmonic oscillator and are given by [28, 29]

$$\langle n|m_x \rangle = d_{m_x, n-j}^j(\pi/2) \approx (-1)^n j^{-1/4} u_n \left( \sqrt{j} \arcsin(m_x/j) \right), \quad (25)$$

where  $u_n(x)$  is the  $n$ th eigenfunction of the harmonic oscillator. Figure 4 presents the overlap of the Fock state  $n = 7$  with the dressed basis  $m_x$ ,  $\langle n = 7|m_x \rangle$ . The overlap is seen to fit Eq. (25) remarkably well. Using the symmetry  $d_{m, m'}^j = (-1)^{m-m'} d_{-m, -m'}^j$  we find that  $(-1)^{n-j-m_x} \langle N - n | -m_x \rangle = \langle n|m_x \rangle$  for all  $m_x$ . This reflects the symmetry  $0 \leftrightarrow \mathbf{k}_B$  in  $H_{2W}^{res}$ .

## B. Detuning

Next, we describe the case in which there is a detuning between the Bragg frequency and the difference in the energy of the momentum modes. We therefore add the detuning to  $H_{2W}$  as we did in Eq. (16). In the matrix (18), a term  $-n\hbar\delta$  is added to the  $n$ th element

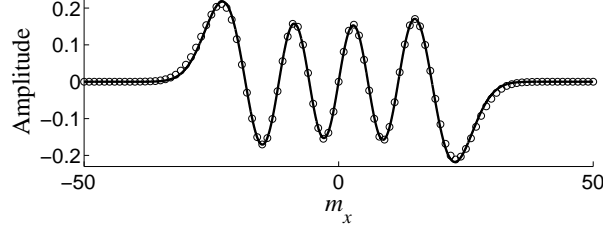


FIG. 4: The overlap between the Fock state  $n = 7$  and the dressed state of  $H_{2W}^{res} m_x$ ,  $\langle n = 7 | m_x \rangle = (-1)^{n-j-m_x} \langle n = N - 7 | -m_x \rangle$  for  $N = 100$ . The harmonic oscillator approximation given by Eq. (25) (line) is seen to be a good approximation.

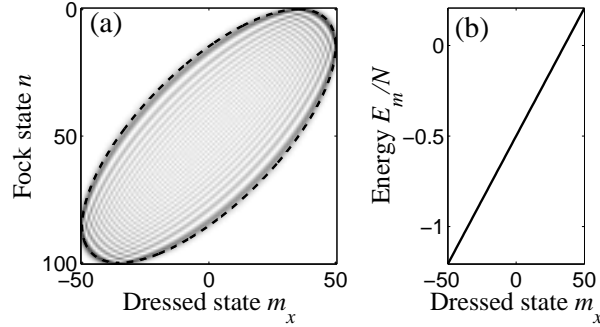


FIG. 5: (a) Absolute value squared of the transformation matrix between the Fock basis and the dressed basis of  $H_{2W}$ ,  $|\langle n | m_x \rangle|^2$ , for  $N = 100$  and  $\delta = \Omega$ . Dashed line is the shape  $(n - j - (\delta/\Omega)m_x)^2 + m_x^2 = j^2$ , which is the generalization of the shape in Fig. 3(b). The spectrum of  $H_{2W}$ , which is again strictly linear, with slope  $\sqrt{\Omega^2 + \delta^2}$ , centered at  $-j\hbar\delta$ . Energy is in units of  $\hbar\Omega$ .

on the main diagonal of the Hamiltonian. The matrix is diagonalized by the transformation matrix shown in Fig. 5 along with the spectrum of the Hamiltonian (16) for  $N = 100$  and  $\delta = \Omega$ . Again, the linear spectrum reflects the single particle nature of the Hamiltonian.

In order to analytically solve Hamiltonian (16) we use the fact that  $\hat{n}_{\mathbf{kB}} = N/2 + \hat{J}_z = j + \hat{J}_z$ , to write  $H_{2W}$  in the angular momentum representation as

$$H_{2W} = \hbar\Omega\hat{J}_x - \hbar\delta\left(\hat{J}_z + j\right) = \hbar\sqrt{\Omega^2 + \delta^2}\hat{J}_l - j\delta. \quad (26)$$

The energy spectrum is again linear, with a spacing of  $\hbar\sqrt{\Omega^2 + \delta^2}$ , centered about  $-j\delta$ . The eigenstates are those of a spin component operator pointing in the  $l$  direction in the  $x - z$  plane, the angle from the  $z$  axis being  $\theta = \pi + \arctan(\Omega/\delta)$ . Thus the transformation matrix

is once again a rotation by  $\theta$  about the  $y$  axis. The shape of the transformation matrix is again captured by classical reasoning (dashed line in Fig 5a).

Dynamics are also easily understood in the angular momentum picture, in terms of spin precession. The Fock basis is characterized by a quantization axis pointing up on the Bloch sphere, while the dressed basis has the quantization axis tilted by an angle  $\theta$  towards the  $x$  axis. This gives a visual understanding of the transformation matrix, as well as the dynamics. The pseudospin evolves by precession about the axis  $l$ , with frequency  $\sqrt{\Omega^2 + \delta^2}$ . The well known properties of Rabi oscillations are obtained in a straight-forward manner. Inversion can only be achieved when the driving field is resonant to the transition between the two modes. As the detuning increases, the amplitude of oscillation decreases and the frequency, which is simply the energy difference between dressed states increases. Since we have neglected interactions, the spectrum is strictly linear, and there is no dephasing.

As in the resonant case discussed in section III A, the symmetry of the rotation matrix allows us to relate the row  $n$  to  $N - n$ . For small  $n$ , both are approximated by properly translated and stretched harmonic oscillator wavefunctions [28].

### C. Rabi oscillations of interacting atoms

Upon inclusion of interactions between the atoms, the problem ceases to be a single body problem, and the second quantization method reviewed in the previous sections becomes useful. The inclusion of interactions in the resonant Bragg coupling of Eq. (17) is correct in the limit  $\mathbf{k}_B \xi > 1$  as discussed in section II B. In this subsection we assume for simplicity  $\delta = 0$ . Generalization to non-resonant Bragg coupling is trivial.

In the angular momentum representation, the interaction term in Eq. (17) can be rewritten up to a constant which we neglect in the form

$$H_{2W}^{int} = \hbar \Omega \hat{J}_x + (\mu/N) \hat{J}_z^2. \quad (27)$$

The transformation matrix obtained by numerically diagonalizing  $H_{2W}^{int}$  is shown along with the obtained spectrum in Fig.6 for  $\mu = \hbar \Omega / 2$ .

The interactions are seen to change the circular shape of the transformation matrix to an oval shape, breaking the symmetry  $m_x \leftrightarrow -m_x$ . The spectrum which is no longer linear indicates this is not a single particle problem.

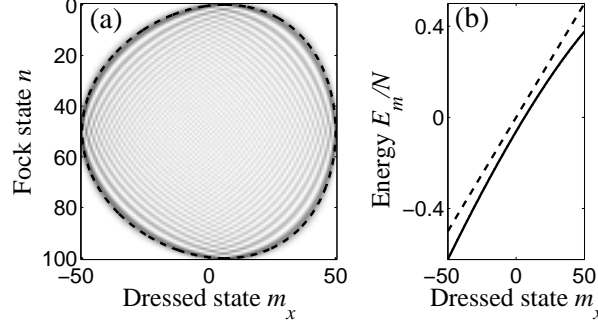


FIG. 6: (a) Absolute value squared of the transformation matrix elements, for  $H_{2W}^{int}$  with  $\mu = \hbar\Omega/2$  and  $N = 100$ . The dashed line is the perturbative classical solution  $m_x = \pm\sqrt{j^2 - m_z^2} + \mu m_z^2/4j$ . (b) The spectrum (solid line) is no longer linear. The non-interacting spectrum is shown for reference as a dashed line. The first order perturbation of Eq. (29) is indistinguishable from the solid line. Energy is in units of  $\hbar\Omega$ .

In order to describe analytically the effect interactions have on the dynamics, we use first order perturbation theory to calculate the energy correction to the state  $|m_x\rangle$ . We start with the eigen-energies of the non-interacting case  $E_{m_x}^{(0)} = \hbar\Omega m_x$ , and add the correction

$$E_{m_x}^{(1)} = \langle m_x | H_{int} | m_x \rangle = -\langle m_x | \frac{\mu}{N} \hat{J}_z^2 | m_x \rangle = \frac{\mu}{2j} \langle m_x | \frac{\hat{J}_x^2 - j(j+1)}{2} | m_x \rangle \quad (28)$$

The overall energy of the state  $|m_x\rangle$  is therefore

$$E_{m_x} = \mu \frac{j-1}{4} + \hbar\Omega m_x + \frac{\mu}{4j} m_x^2. \quad (29)$$

This perturbative result for the spectrum is indistinguishable from the solid line in Fig. 6b which is obtained by exact diagonalization. The dashed line in Fig. 6(a) is a perturbative correction to that of Fig. 3(a). It is derived by assuming the energy is nearly linear, and therefore  $(\mu/\hbar\Omega)m_z^2/4j$  is added to  $m_x$ . This line is seen to indeed describe the peak amplitudes of the transformation matrix very well.

The departure of the energy spectrum from a linear one, as shown in Fig 6b, leads to a dephasing between the different dressed states. According to Eq. (25), an initial Fock state  $n = 0$  is a gaussian with width  $\sqrt{j}$ . Hence a collapse should occur at a time scale over which a  $\pi$  phase is acquired in the quadratic terms of the energies of the states  $m_x = 0$  and  $m_x = \sqrt{j}$ . According to Eq. (29) this energy is  $\mu/4$ , leading to a collapse time of  $t_{collapse} = 4\pi\hbar/\mu$ . In Fig 7, we see the decaying oscillations due to the perturbative dynamics governed by Eq.



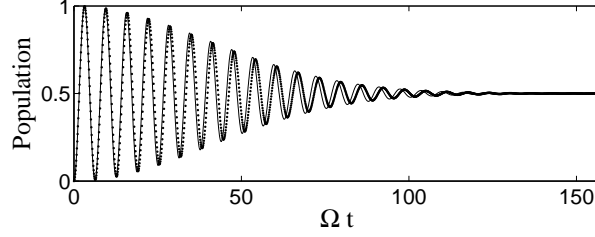


FIG. 7: The expectation value for population of mode  $\mathbf{k}_B$  evolving according to  $H_2W^{int}$  with interactions for  $\mu = \hbar\Omega/2$ , and  $N = 100$ . The dots are according to the numerical diagonalization of  $\hbar\Omega/2\hat{J}_x + \mu/N\hat{J}_z^2$ . The line is according to  $H_2W$  with the first order correction to the energies (29).

(29) fit the exact numerical solution remarkably well. A revival occurs when each quadratic phase is a multiple of  $2\pi$ . This happens for multiples of the  $t_{revival} = 4\pi\hbar N/\mu$ . In realistic experimental conditions,  $N$  is typically on the order of  $10^5$  and thus decoherence is likely to occur much before  $t_{revival}$  and we do not expect revivals to be seen.

The broadening in the spectrum which causes  $t_{collapse}$  is proportional to the chemical potential, and exists for a spatially homogeneous system. It should not be confused with the broadening in the resonance of Bogoliubov quasiparticles over a spatial inhomogeneous BEC, known as inhomogeneous broadening [30], where the local density gives rise to a local chemical potential and a local mean-field shift. For rapid Rabi oscillations this well known inhomogeneous broadening is suppressed [19]. The slow decay discussed here is due to a *temporal* inhomogeneity, rather than a spatial inhomogeneity in the mean-field energy. The origin of this decay is in the spread of dressed states spanning the initial state  $m_z = -j$ , each having a slightly different Rabi frequency. The decay can be explained in the Bloch sphere picture by a spread in the initial conditions due to quantum uncertainty. The initial state  $m_z = -j$  is classically described as a vector pointing down on a Bloch sphere of radius  $j$ . However this is only the expectation value of the angular momentum, and there is a fluctuation (independent of  $j$ ) in the initial value of  $j_x$  and  $j_y$ . This uncertainty in the initial conditions exists in the linear Rabi oscillation problem too, but all vectors have the same oscillation frequency, thus all possible vectors return to their initial value together and there is no dephasing. Non-linearity causes the different trajectories to have a slightly different Rabi frequency, thus causing dephasing. This decay is therefore not predicted by

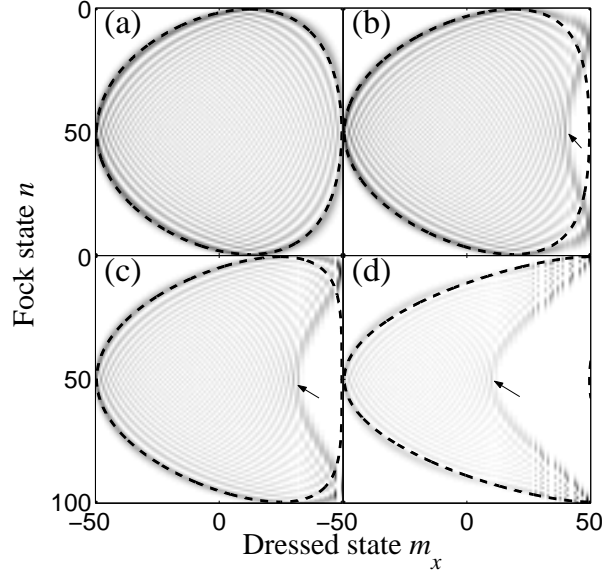


FIG. 8: The transformation matrices of  $H2W^{int}$  for different values of  $\mu/\hbar\Omega = 1, 1.5, 2$  and  $4$  (a-d respectively). For  $\mu < \hbar\Omega$  the perturbative classical equation  $m_x = \pm\sqrt{j^2 - m_z^2} + (\mu/\hbar\Omega)m_z^2/4j$  describes the region of high amplitude in the transformation matrix quite well (dashed line). This approximation breaks down as the instability comes in. At  $\mu = 2\hbar\Omega$ , the turning point reaches the initial dressed state vector, when starting from the  $n = 0$  Fock state, and the dynamics depart from the perturbative expectation (see Fig. 9)

the homogeneous Gross-Pitaevskii equation, which corresponds to a single trajectory of the expectation value of  $\mathbf{j}$  on the Bloch sphere.

The perturbative treatment discussed above is correct for  $\mu < \hbar\Omega$ . It is known that for  $\mu = \hbar\Omega$  a dynamical instability occurs in the solution of the two mode Gross-Pitaevskii equation [18]. In our model the signature of the instability is manifested by the deviation of the region of high amplitude in the transformation matrix from the oval shape, as seen in Fig. 8. For  $\mu = \hbar\Omega$  the perturbative classical fit to the shape of the transformation matrix is still good, and the curvature of both vanish at  $m_x = j$  (Fig. 8a). For  $\mu > \hbar\Omega$  the transformation matrix becomes concave (Fig. 8b). The right hand side of the transformation matrix varies greatly from the corresponding perturbative result, while the left hand side is seen to follow the perturbative shape even for  $\mu > \hbar\Omega$ .

We find numerically that for  $m_x$  larger than a critical  $m_x^c$ , the energy is doubly degenerate, with one corresponding eigenvector located only in the top half of the matrix ( $n < j$  or

$m_z < 0$ ), and the other located in the bottom of the matrix ( $n > j$  or  $m_z > 0$ ). The value of  $m_x^c$  is found to decrease towards the turning point in the transformation matrix (arrows in Fig. 8b-d) as the matrix size  $N$  is increased. Thus we conclude that in the thermodynamic limit  $m_x^c$  coincides with the turning point in the shape of the matrix.

To the left of the instability, eigenvectors have nonvanishing amplitudes both in the upper and the lower half of the transformation matrix. An initial state that spans a number of such eigenvectors is able to perform Rabi oscillations. The accumulated phases cause alternating constructive and destructive interferences for a large range of  $n$ . To the right of the instability this is not the case. In the thermodynamic limit, each eigenvector is located completely either in the top half or in the bottom half of the matrix. Therefore all eigenvectors spanned by a state in the upper half will always interfere in the upper half and  $n > j$  will never be reached. Thus in this region inversion is impossible, an effect known as macroscopic self-trapping [31].

The Fock state  $n = 0$  is approximated by a Gaussian superposition of dressed states of width  $\sqrt{j}$ , centered at  $(\mu/\hbar\Omega)j/4$ . For  $\mu = 2\hbar\Omega$ , the point of instability is found to reach  $\mu j/4$ . Thus as  $\mu$  approaches  $2\Omega$ , the point of dynamic instability reaches the trajectory of the initial Fock state  $n = 0$ . Fig. 9 shows the time dynamics of the initial condition  $n = 0$  for the same ratios of  $\mu/\hbar\Omega$  as in Fig. 8. For  $\mu < 2\hbar\Omega$ , we see Rabi oscillations. Even though there is a turning point (in Fig. 8b), as long as it is not on the eigenstates occupied by  $n = 0$ , oscillations are regular. For  $\mu \approx 2\hbar\Omega$  (Fig. 8c), the oscillations decay rapidly, and there is a noisy fluctuation with no clear frequency in the population of  $n$ . Finally, for  $\mu > 2\hbar\Omega$  we see the macroscopic self-trapping (Fig. 8d).

In the next section we move on to describe three-wave mixing with the tools developed in this section. The three-wave Hamiltonian derived in section II A describes interactions also in the low  $k$  limit, but are limited to weak excitations which do not deplete the macroscopically occupied mode.

#### IV. THREE-WAVE MIXING

In this section we discuss three-wave mixing of Bogoliubov quasiparticles, as governed by the Hamiltonian in Eq. (13). In the limit of large momentum, where the quasiparticle operators  $\hat{b}_{\mathbf{k}}$  coincide with the atomic operators  $\hat{a}_{\mathbf{k}}$ , the three-wave mixing described

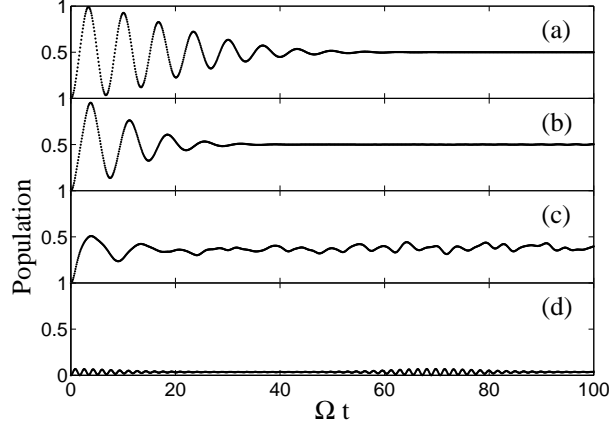


FIG. 9: The expectation value for population of state  $\mathbf{k}_B$  as a function of time for the same parameters as in fig 8. For  $\mu < 2\hbar\Omega$  the dynamics are described quite well by the perturbative treatment (a,b). As  $\mu$  approaches  $2\hbar\Omega$ , the turning point in Fig. 8(c) reaches the initial dressed states and the dynamics become unstable (c). For  $\mu > 2\hbar\Omega$  (d), we find weak oscillations which cannot reach inversion (macroscopic self-trapping).

here corresponds to four-wave mixing of atomic matter waves [7]. The fourth wave is the condensate which is the vacuum of the Bogoliubov quasiparticles. In the limit of low momentum, the four-wave picture is incorrect, as each quasiparticle mode  $\hat{b}_{\mathbf{k}}$  is a superposition of atomic operators with momenta  $\hbar\mathbf{k}$  and  $-\hbar\mathbf{k}$ . This Hamiltonian does not conserve the total number of excitations  $n_{\mathbf{k}} + n_{\mathbf{q}} + n_{\mathbf{k}-\mathbf{q}}$ , indicating these excitations are not particles, but rather quasiparticles whose number need not be conserved. There are two independent conserved quantities  $M = n_{\mathbf{q}} - n_{\mathbf{k}-\mathbf{q}}$ , and  $N = n_{\mathbf{k}} + n_{\mathbf{k}-\mathbf{q}}$ , which lead to the possibility of diagonalizing a subspace of Eq. (13) with only one quantum number  $n = n_{\mathbf{k}-\mathbf{q}}$  representing the Fock state  $|(N - n)_{\mathbf{k}}, (M + n)_{\mathbf{q}}, n_{\mathbf{k}-\mathbf{q}}\rangle$ , where  $n$  varies between 0 and  $N$ . The fact that the difference in the occupation of modes  $\mathbf{q}$  and  $\mathbf{k} - \mathbf{q}$  is constant can be used as a source of number-squeezed states. In the low momentum regime suggested here, dephasing is slow and pair correlated atomic beams should be easier to generate than in the high momentum regime studied experimentally in [3].

### A. Resonant three-wave mixing

We consider first the resonant case  $\Delta = 0$  of Eq. (11), where the sum of energies of the quasiparticle modes  $\mathbf{q}$  and  $\mathbf{k} - \mathbf{q}$  is equal to the energy of mode  $\mathbf{k}$ , i.e.  $\epsilon_k = \epsilon_{\mathbf{q}} + \epsilon_{|\mathbf{k}-\mathbf{q}|}$ . The modes  $\mathbf{q}$  and  $\mathbf{k} - \mathbf{q}$  are thus on the energy-momentum conserving surface for Beliaev damping from mode  $\mathbf{k}$  as shown in Fig. 2a.  $H_{3W}$  couples between pairs of modes in this subspace which have a difference of 1 in  $n$ , and can be represented by the  $(N+1) \times (N+1)$  tri-diagonal matrix

$$H_{3W}^{res} = \frac{K}{2} \begin{pmatrix} 0 & \sqrt{(N-0)M} & 0 & \dots & & \\ \sqrt{(N-0)M} & 0 & \sqrt{(N-1)2(M+1)} & & & \\ 0 & \sqrt{(N-1)2(M+1)} & 0 & & \ddots & \\ \vdots & & \ddots & \ddots & \ddots & \sqrt{N(M+N)} \\ & & & \sqrt{N(M+N)} & 0 & \end{pmatrix} \quad (30)$$

with a coupling term  $K = g\sqrt{N_0}A_{\mathbf{k},\mathbf{q}}/V = \mu A_{\mathbf{k},\mathbf{q}}/\sqrt{N_0}$ . When  $H_{3W}^{res}$  is diagonalized, we get a new set of  $N+1$  eigenstates, dressed by interactions,  $|m_x\rangle$ , where  $m_x$  varies between  $-N/2$  and  $N/2$ .

The square of the transformation matrix elements are shown in Fig. 10 for  $N = 100$ ,  $M = 50$  along with the eigen-energies. As can be seen by comparison with Fig. 3, the spectrum and the transformation matrix seem similar to those of  $H_{2W}^{res}$ . In fact, as the seed  $M$  is taken to be larger than  $N$ , the factor  $\sqrt{M+n}$  becomes more uniform, and can be taken out of the matrix (30) as a multiplicative factor. Thus in the limit  $M \gg N$ , both transformation matrix and eigenvalues are well approximated by the two-wave mixing solution described in section III, with  $\hbar\Omega \approx K\sqrt{M}$ .

Even when  $M$  is smaller than  $N$  (but still large enough to seed mixing), the factors originating from the  $\mathbf{k} - \mathbf{q}$  amplitudes in adjacent matrix elements of  $H_{3W}$ , are almost the same,  $\sqrt{M+n} \approx \sqrt{M+n+1}$ . We use this to approximate Eq. (30) *locally* as a two-wave mixing Hamiltonian multiplied by a local  $\sqrt{M+n}$ .

The transformation matrix in Fig. 10(a) is indeed very well approximated by stretching the  $n$ 'th line of the rotation matrix (Fig. 3(a)) by a factor  $\sqrt{M+n}/\sqrt{M+\bar{n}}$ .  $\bar{n}$  is the  $n$  for which the derivative of  $\sqrt{N-n}\sqrt{M+n}\sqrt{n}$  with respect to  $n$  vanishes. For  $M \gg N$  the

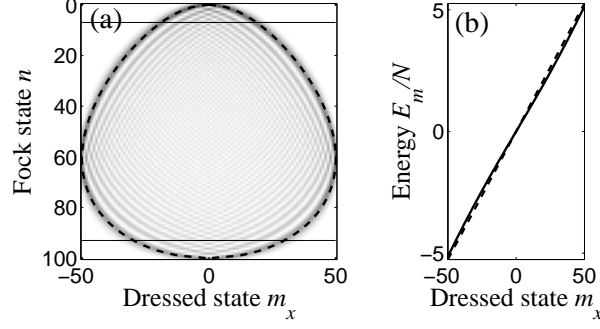


FIG. 10: (a) Absolute value squared of transformation matrix of  $H_{3W}^{res}$  (Eq. (11)) for  $N = 100, M = 50$  and  $\Delta = 0$ . The thin lines are at the rows  $n = 7$  and  $N - 7$ . The dashed line is the line  $m_x^2 + m_z^2 \times (M + n)(M + \bar{n}) = j^2$ . (b) The exact spectrum (solid line) of  $H_{3W}^{res}$  linearly approximated by  $\sqrt{M + \bar{n}} m_x$  (dashed line). Energy is in units of  $K$ . The second order perturbation approximation (Eq. 33) is indistinguishable from the solid line.

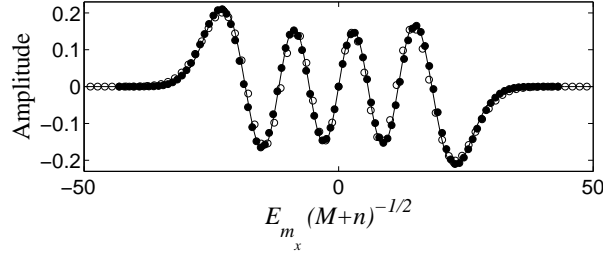


FIG. 11: The  $n = 7$  (filled circles) and the  $n = N - 7$  (empty circles) rows of the transformation matrix presented in Fig. 10(a), divided by  $\sqrt{M + n}$ . The x axis is the energy as calculated by Eq. (33), and divided by  $\sqrt{M + n}$ . The amplitudes of the different Fock states are normalized by  $[(M + n)/(M + \bar{n})]^{1/4}$ . The line is the same function (Eq. 25) as in the two-wave mixing in Fig. 4.

approximation of  $H_{3W}^{res} = H_{2W}^{res}$  becomes exact.

As can be seen in Fig. 11, for small  $n$ , both rows  $n$  and  $N - n$  agree remarkably well with the function (25) when plotted versus the spectrum of  $H_{3W}^{res}$ , as in the case of two-wave mixing, even for  $M < N$ .

The spectrum is nearly linear centered around 0 with a slope  $dE = K\sqrt{M + \bar{n}}$ . This leads to oscillations, with oscillation period of  $t = h/dE$  in analogy to the two-wave mixing case. These oscillations decay due to the fact that the spectrum is not strictly linear. In order

to model analytically the nonlinearity in the spectrum, we replace both operators  $\hat{b}_{\mathbf{q}}$  and  $\hat{b}_{\mathbf{q}}^\dagger$  by the operator  $\sqrt{M + \hat{b}_{\mathbf{k}-\mathbf{q}}^\dagger \hat{b}_{\mathbf{k}-\mathbf{q}}}$  where the square root of an operator is determined by a Taylor expansion. Since in the Hamiltonian (11)  $\hat{b}_{\mathbf{q}}$  commutes with  $\hat{b}_{\mathbf{k}}^\dagger \hat{b}_{\mathbf{k}-\mathbf{q}}$ , we approximate Eq. (11) in a symmetric form:

$$H_{3W}^{res} \approx \frac{K}{2} \left( \sqrt{M + \hat{b}_{\mathbf{k}-\mathbf{q}}^\dagger \hat{b}_{\mathbf{k}-\mathbf{q}}} \hat{b}_{\mathbf{k}}^\dagger \hat{b}_{\mathbf{k}-\mathbf{q}} + \hat{b}_{\mathbf{k}} \hat{b}_{\mathbf{k}-\mathbf{q}}^\dagger \sqrt{M + \hat{b}_{\mathbf{k}-\mathbf{q}}^\dagger \hat{b}_{\mathbf{k}-\mathbf{q}}} \right). \quad (31)$$

We now define angular momentum operators in complete analogy to Eqs. (19-23) with the substitution  $\hat{a}_{\mathbf{kB}} \rightarrow \hat{b}_{\mathbf{k}-\mathbf{q}}$  and  $\hat{a}_0 \rightarrow \hat{b}_{\mathbf{k}}$ . In the angular momentum representation Eq. (31) becomes

$$H_{3W}^{res} \approx \frac{K}{2} \left( \sqrt{M + j + \hat{J}_z} \hat{J}^+ + \hat{J}^- \sqrt{M + j + \hat{J}_z} \right). \quad (32)$$

To the lowest order in  $\hat{J}_z/(M + j)$  we have  $H_{3W}^{res} \approx \hbar \bar{\Omega} \hat{J}_x$  which is simply  $H_{2W}^{res}$  in Eq. (24), where  $\hbar \bar{\Omega} = K \sqrt{M + j}$ . We use perturbation theory to second order in  $\hat{J}_z/(M + j)$ , to find the corrections to the energy due to the non-linearity.

$$E_{m_x} = \hbar \bar{\Omega} \left[ \left( 1 - \frac{j(j+1)}{16(M+j)^2} \right) m_x + 5 \frac{m_x^3}{16(M+j)^2} \right], \quad (33)$$

The perturbative spectrum obtained in Eq. (33) is indistinguishable from the solid line in Fig. 10(b).

As in the nonlinear case studied in section III C, the nonlinearity in the spectrum leads to dephasing in the dynamics. Fig. 12 compares between the numerical (a) and the perturbative (b) results of the population of mode  $\mathbf{k} - \mathbf{q}$  vs. time, with the initial condition  $n_{\mathbf{k}-\mathbf{q}} = 0$ . It is seen that the perturbative solution captures the non-linear dynamics quite well even for  $M < N$ . The rapid oscillation at frequency  $dE/h$  are unresolved in Fig. 12, but the envelope is seen to be in good agreement. As expected from wave mixing, there are oscillations between the population of the quasiparticle modes  $\mathbf{k}$  and  $\mathbf{k} - \mathbf{q}$ . The seed in mode  $\mathbf{q}$  oscillates as well and has the occupation  $M + n$ . The initial Fock state is a gaussian superposition of dressed states of width  $\sqrt{jM/(M + \bar{n})}$ , thus the decay time is approximated analytically by  $t_{decay} = h/E \sqrt{jM/(M + \bar{n})} \sim \frac{32\pi\sqrt{j}}{5\Omega}$  in agreement with Fig. 12. There is a revival after time  $t_{revival} \propto N$ , due to the finite number of quasiparticles. This revival time however is much longer than the decoherence time for realistic values of  $N$ . Note that as opposed to the interacting Rabi oscillating atoms of section III C, in which oscillation period and decay time are independent of  $N$ , both times obtained from Eq. (33) scale as  $\sqrt{j}$ , when the ratio

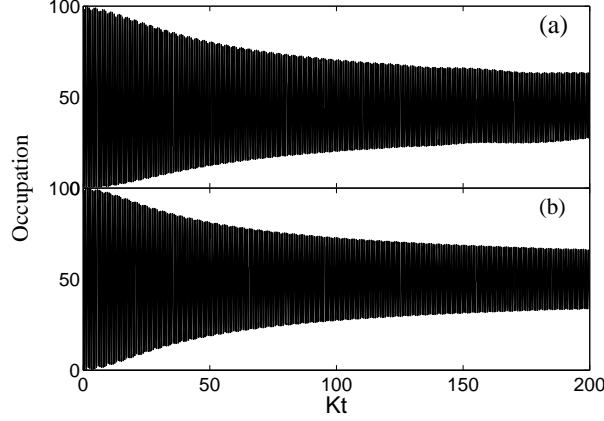


FIG. 12: The expectation value of the occupation of mode  $\mathbf{k} - \mathbf{q}$  as a function of time obtained by numerical diagonalization (a) and perturbative calculation (b) of  $H_{3W}^{res}$ , for the same parameters as in Fig. 10, and starting with the Fock state  $n = 0$ . Time is in units of  $\hbar/K$ .

$M/2j$  is kept constant. Solving for a large system of size  $j$ , would require the diagonalization of matrices of size  $2j + 1$ . An approximate solution therefore can be attained by solving for moderate  $j'$  and scaling the result by  $\sqrt{j/j'}$ .

## B. Detuning

In the previous subsection, the seed, mode  $\mathbf{q}$ , was on the energy-momentum conserving surface of mode  $\mathbf{k}$ . Exact energy conservation is not a necessary condition for wave mixing as also a populated mode with a small detuning  $\Delta$  from this surface, as shown in Fig. 2b will lead to wave mixing. Figure 13 shows the dressed state spectrum obtained by numerical diagonalization of  $H_{3W}^{res}$  (Eq. (13)) at different detunings for  $N = 10$  and  $M = 5$ .

When a detuning term is added to  $H_{3W}$ , Eq. (32) is modified to

$$H_{3W} \approx \frac{K}{2} \left( \sqrt{M + j + \hat{J}_z \hat{J}^+} + \hat{J}^- \sqrt{M + j + \hat{J}_z} \right) + \hbar \Delta (j + \hat{J}_z). \quad (34)$$

A perturbative approximation to the energy spectrum is obtained in a similar fashion to Eq. (33), with the Hamiltonian (34) and is indistinguishable from the solid lines in Fig. 13. At detunings much larger than  $K/\hbar$ , the Hamiltonian (34) is nearly diagonalized in the Fock basis  $n$  or  $m_z = n - j$ . The energy spacing, and therefore the energy span of the spectrum, increases linearly with the detuning. At large negative detunings, the lowest



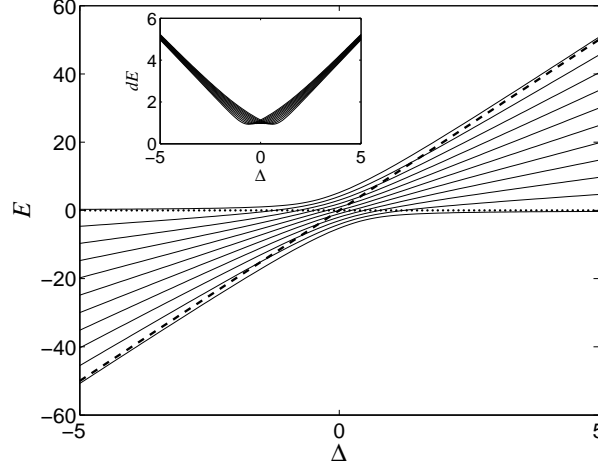


FIG. 13: The spectrum of  $H_{3W}$  for  $N = 10$  and  $M = 5$  vs. detuning. Detuning is in units of  $\bar{\Omega}$ , and energy in units of  $\hbar\bar{\Omega} = K\sqrt{M+j}$ . The perturbative result is indistinguishable from the exact calculation (solid line). Dashed line is  $E = N\hbar\Delta$ , the lowest (largest) energy for large negative (positive) detuning. Dotted line is  $E = 0$ . For large negative detuning, the lowest dressed state corresponds to the initial state  $n = N$ , while for large positive detuning, the lowest dressed state corresponds to  $n = 0$ . By adiabatically sweeping the detuning, one can transfer all population from modes  $\mathbf{k}$  and  $\mathbf{k} - \mathbf{q}$  to modes  $\mathbf{q}$  and  $\mathbf{k} - \mathbf{q}$ . The inset is the difference between adjacent eigenenergies. Non-linearity initially increases with  $|\Delta|$ , reaches a maximum which depends weakly on  $M/N$  and is always at  $|\Delta| \approx \bar{\Omega}$ , and then decreases for large  $|\Delta|$ .

energy dressed state corresponds to the Fock state where all of the excitations are in modes  $\mathbf{k}$  and  $\mathbf{q}$ , whereas at large positive detunings the lowest energy dressed state corresponds to the Fock state where all of the excitations are in modes  $\mathbf{q}$  and  $\mathbf{k} - \mathbf{q}$ . In analogy to rapid adiabatic passage between two atomic levels, using a sweep in the laser frequency, an adiabatic transfer of the excitations population between the excitation modes of a BEC is possible using a sweep in the detuning. Given an initial state where all of the excitations in modes  $\mathbf{k}$  and  $\mathbf{q}$  at a large negative detuning, an adiabatic sweep of the detuning to a large positive value, would adiabatically transfer all of the excitations into modes  $\mathbf{q}$  and  $\mathbf{k} - \mathbf{q}$ . A possible way to sweep the detuning during the experiment would be the use of a magnetic Feshbach resonance to tune  $g$  [32].

In analogy with Eq. (16), we find that to zero order in  $\hat{J}_z/(M+j)$ ,  $H_{3W}$  in Eq. (34) is given by  $H_{3W}^{(0)} = \hbar\sqrt{\Omega^2 + \Delta^2}\hat{J}_l$ , where the axis  $l$  points in an angle  $\theta = \pi + \arctan(\bar{\Omega}/\Delta)$  from

the  $z$  axis in the  $x - z$  plane. For nonzero detuning the first order perturbative correction to the dressed states' energies is proportional to  $\hat{J}_z/(M + j)$ . Therefore as the detuning is increased from zero, the spread in the differences between adjacent dressed states energies (non-linearity in the spectrum) is expected to grow. On the contrary, for large detuning Eq. (34) is dominated by the last term and  $H_{3W}^{(0)}$  is proportional to  $|\Delta|$ , so the spectrum approaches the linear spectrum of two-wave mixing with large detuning. This is simply the zeeman shift in the angular momentum representation. We therefore expect there will be an intermediate value of detuning for which the spread in energy differences will be maximal. The inset of Fig. 13 shows the energy difference between adjacent dressed states for the same parameters as in the main figure. The non-linearity of the spectrum indeed increases initially with the detuning, due to the quadratic nonlinearity which is added in the presence of detuning, and decreases towards  $\Delta$  for large  $|\Delta|$ .

The spread in energy differences is manifested as dephasing in the dynamics of the system. Figure 14 shows  $\langle \hat{b}_{\mathbf{k}-\mathbf{q}}^\dagger \hat{b}_{\mathbf{k}-\mathbf{q}} \rangle$  as a function of time, for three different detuning values,  $\Delta = 0$  (dotted line),  $\Delta = \bar{\Omega}$  (dashed line) and  $\Delta = 3\bar{\Omega}$  (solid line), beginning from the initial state  $|n_{\mathbf{k}} = N, n_{\mathbf{q}} = M, n_{\mathbf{k}-\mathbf{q}} = 0\rangle$  with  $N = 100$  and  $M = 50$ . The oscillation frequency is found to increase with detuning to a value of  $\Omega_{eff} \equiv \sqrt{\bar{\Omega}^2 + \Delta^2}$ . The oscillations amplitude is seen to decrease with larger detuning as  $1/\Delta^2$ . The decay time of oscillations initially increases, and then decreases, in agreement with the spread in the energy differences plotted in the inset of Fig. 13, for which the maximal spread is for  $\Delta/\bar{\Omega} \approx 1.5$ . We use perturbation theory, in analogy to Eq. (32), to calculate the spectrum and  $t_{decay}$  in the presence of detuning. These perturbative results are found to fit the exact solution very well.

## V. BELIAEV DAMPING

Thus far we have discussed the time evolution of the system within the dressed state subspace, which is defined by the initial population of the  $\mathbf{k}$  and  $\mathbf{q}$  modes, and have neglected damping into empty modes. In analogy to the treatment of spontaneous photon scattering as a transfer between dressed state subspaces of an atom interacting with a laser field [16], we now consider scattering into empty modes as transfer between dressed state subspaces. The damping of excitations from the mode  $\mathbf{k}$  is no longer elastic, but rather carries the energy difference between the dressed states among which it occurred. The extra energy is taken

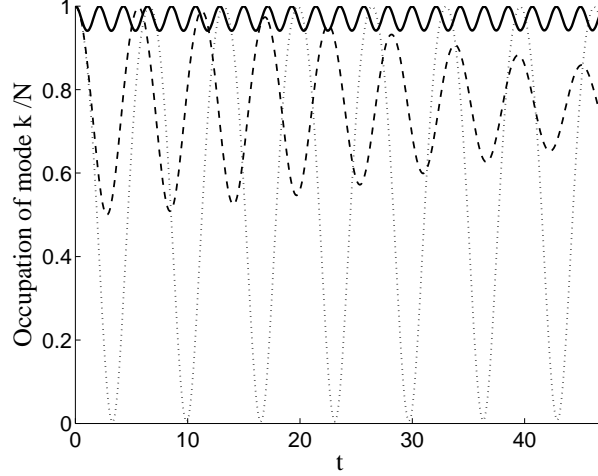


FIG. 14: The expectation value of the occupation of mode  $\mathbf{k}$  as a function of time, for three different detuning values,  $\Delta = 0$ ,  $\Delta = \bar{\Omega}$  and  $\Delta = 3\bar{\Omega}$  (dotted, dashed and solid lines respectively) for  $N = 100$  and  $M = 50$ . The oscillation decay time for  $\Delta = \bar{\Omega}$  is much shorter than for  $\Delta = 0$  and  $\Delta = 3\bar{\Omega}$ , in agreement with the energy differences in the dressed state spectra for the these detunings (see inset of Fig. 13). Time is in units of  $1/\bar{\Omega}$ .

from the interaction between the wave packets in the  $\mathbf{k}$  and  $\mathbf{q}$  modes and was initially put into the system by the lasers which excited the condensate into the  $(N, M)$  subspace. We consider only damping from the momentum mode  $\mathbf{k}$  since the damping rate from momentum modes  $\mathbf{q}$  and  $\mathbf{k} - \mathbf{q}$  is typically much smaller [15].

The damping is an irreversible process due to the quasi-continuum of  $N_c$  modes  $\mathbf{q}'$  (other than  $\mathbf{q}$  and  $\mathbf{k} - \mathbf{q}$ ) on the energy-momentum conserving surface. The transition amplitudes between all possible pairs of dressed states under

$$H_{damping} = \frac{g}{2V} \sqrt{N_0} \sum_{\mathbf{q}' \neq \mathbf{q}, \mathbf{k} - \mathbf{q}} A_{\mathbf{k}, \mathbf{q}'} \left( \hat{b}_{\mathbf{q}'}^\dagger \hat{b}_{\mathbf{k} - \mathbf{q}'}^\dagger \hat{b}_{\mathbf{k}} \right), \quad (35)$$

reveal the spectral structure of the damping process.

The decay from mode  $\mathbf{k}$  decreases  $N$  by 1 and does not change the value of  $M$ , Hence in the angular momentum representation, a dressed state  $|j, m_x\rangle$  can decay into  $|j - 1/2, m'_x\rangle$ . The matrix elements of the Hamiltonian  $H_{damping}$  between numerically obtained eigenstates of  $H_{3W}$  (Eq. 13)  $\langle j - 1/2, m'_x | H_{damping} | j, m_x \rangle$ , are plotted in Fig. 15(a) as a function of the energy difference between the states  $E_{m_x} - E_{m'_x}$  for  $N = M = 10, \Delta = 0$ . Transition amplitudes are large only between dressed states of neighboring energies in the two

subspaces. The damping process is schematically shown in Fig. 15(b). Starting from the  $N = M = 10$  subspace with 11 dressed states, Beliaev damping of an excitation from the  $\mathbf{k}$  momentum mode into two empty modes,  $\mathbf{q}'$  and  $\mathbf{k} - \mathbf{q}'$ , will transfer the system into the  $N' = 9, M' = 10$  subspace with 10 dressed states. Since the energy spectrum in both subspaces is nearly linear, and there is one less state in the smaller subspace, the energy differences between states coupled by  $H_{damping}$  are almost the same for all initial dressed states. The decay of each dressed state into only two neighboring states in Fig. 15(b) results in a structure of a doublet in the Beliaev damping spectrum which is plotted in Fig. 16 for experimentally realistic parameters.

We choose as a model system a condensate of  $3 \times 10^5$ ,  $^{87}\text{Rb}$  atoms in the  $F = 2, m_f = 2$  ground state. The condensate, which is similar to the experimental parameters of [33], is homogeneous and has a density of  $3 \times 10^{14}$  atoms/cm<sup>3</sup>. The damping rate per excitation of each transition is taken as a Lorentzian with a width and height of  $\Gamma/N_{\mathbf{k}}$  around  $E_{m_x} - E_{m'_x}$ .  $N_{\mathbf{k}}$  is the average occupation of mode  $\mathbf{k}$  for the dressed state  $|m_x\rangle$ . Averaging over all of the possible transitions between subspaces, weighed by the initial dressed state occupation, Fig. 16 shows the damping rate from the  $N = M = 5 \times 10^3$  to the  $N = 5 \times 10^3 - 1, M = 5 \times 10^3$  subspace vs. energy, for  $k\xi = 3.2$ ,  $q = k/\sqrt{2}$  and  $\Delta = 0$  (solid line). The rates are calculated numerically according to the Fermi golden rule [12]:

$$\Gamma_{m_x, m'_x} = \frac{2\pi}{\hbar} \sum_{\mathbf{q}'} |\langle j - 1/2, m'_x | H_{damping} | j, m_x \rangle|^2 \delta(\epsilon_k + E_{m_x} - \epsilon_q - \epsilon_{\mathbf{k}-\mathbf{q}} - E_{m'_x}). \quad (36)$$

A clear doublet structure is evident. This splitting of the spectrum is analogous to the Autler-Townes splitting where the spectrum of spontaneous emission is split due to rapid Rabi oscillations [34].

Intuitively we expect a doublet in the spectrum to appear as a result of the temporal oscillations in the occupation of mode  $\mathbf{k}$ . The decay from mode  $\mathbf{k}$  is modulated, and the spectrum of a linear system is a Fourier transform of its time correlation function [35]. Temporal modulations, therefore, lead to a splitting of the oscillation frequency in the decay spectrum. This argument is strictly true only for a linear system such as  $H_{2W}$ .

To understand the doublet structure of the decay spectrum, we use the local similarity of  $H_{3W}$  to  $H_{2W}$ , and approximate the three-wave damping rate by the two-wave damping rate. The eigenstates of  $H_{2W}$ ,  $|j, m_x\rangle$  can be viewed as  $N = 2j$  spin 1/2 quanta,  $n_\alpha = j - m_x$  of them pointing in the +x direction (right) and  $n_\beta = j + m_x$  of them pointing in the -x direction

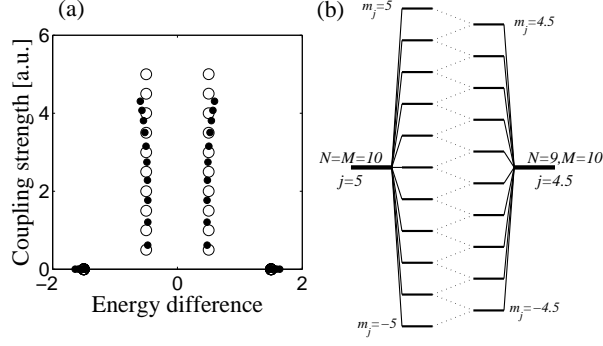


FIG. 15: (a) The strength of coupling between pairs of dressed states in the two subspaces  $N = 10, M = 10$  and  $N' = 9, M = 10$  as a function of the energy difference between the two states. In the linear two-wave approximation (empty circles) the coupling is strictly only to the two states closest in energy, and the coupling strength is linear in  $m_x$  as implied in Eq. (37). For three-wave mixing (filled circles), there is a negligible coupling to other states, and the coupling is no longer linear in  $m_x$ . (b) Schematic drawing of Beliaev damping as transfer between the subspaces.

(left). We use the Schwinger boson mapping (sec. III A) to associate operators  $\hat{\alpha}$  and  $\hat{\beta}$  with  $\hat{J}_x$ . The state  $|j, m_x\rangle$  can be expressed by the quantum numbers  $|n_\alpha, n_\beta\rangle$ , just as the state  $|j, m_z\rangle$  is equivalent to  $|n_{\mathbf{k}}, n_{\mathbf{k}-\mathbf{q}}\rangle$ . The operator  $\hat{b}_{\mathbf{k}}$  which annihilates a spin pointing in the  $+z$  direction is then given by  $\hat{b}_{\mathbf{k}} = 1/\sqrt{2}(\hat{\alpha} - \hat{\beta})$ . We use the Fock representation to write  $(\hat{\alpha} - \hat{\beta})|n_\alpha, n_\beta\rangle = \sqrt{n_\alpha}|n_\alpha - 1, n_\beta\rangle - \sqrt{n_\beta}|n_\alpha, n_\beta - 1\rangle$ . Transforming this to angular momentum quantum numbers using  $n_\alpha = N/2 + m_x = j + m_x$  and  $n_\beta = j - m_x$ , we get

$$\hat{b}_{\mathbf{k}}|j, m_x\rangle \approx \frac{1}{\sqrt{2}} \left( \sqrt{j + m_x} \left| j - \frac{1}{2}, m_x - \frac{1}{2} \right\rangle - \sqrt{j - m_x} \left| j - \frac{1}{2}, m_x + \frac{1}{2} \right\rangle \right). \quad (37)$$

From Eq. (37) it is evident that  $H_{damping}$  couples the dressed state  $|j, m_x\rangle$  only to the two dressed states  $|j - 1/2, m_x \pm 1/2\rangle$ .

We have derived Eq. (37) under the assumption that  $H_{3W}$  is indeed approximated by  $H_{2W}$ . In Fig. 15(a) we see a comparison between the matrix elements of  $H_{damping}$  for numerically obtained dressed states  $|j, m_x\rangle$  (filled circles) and the two-wave approximation (empty circles). The spread in the energy difference is due to the non-linearity in the spectrum of  $H_{3W}$ , however  $H_{damping}$  is found to significantly couple only dressed states with neighboring energies as in the two-wave approximation.

A perturbative result for the decay spectrum where energies are calculated according to

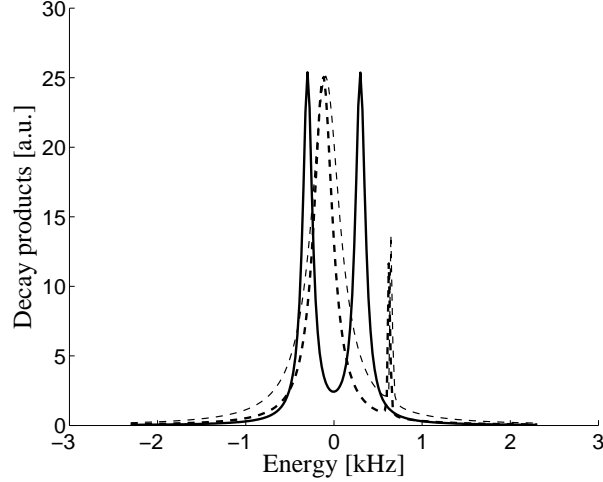


FIG. 16: Damping spectrum between the  $N = M = 5 \times 10^3$  subspace and the  $N = 5 \times 10^3 - 1$ ,  $M = 5 \times 10^3$  subspace, at  $k\xi=3.2$ , and  $q = k/\sqrt{2}$ . For these parameters  $\bar{\Omega} = 2\pi \times 610$  Hz. For  $\Delta = 0$  (solid line), the perturbative result is indistinguishable from the numerically calculated spectrum. For  $\Delta = \bar{\Omega}$  the perturbative result (thin dashed line) is still a reasonable approximation to the numerical calculation (thick dashed line). The calculation was done with  $j = 50$  and scaled to  $j = 2500$ .

Eq. (33) and rates according to Eqs. (36,37) is indistinguishable from the numerical result in Fig. 16 for resonant wave mixing.

Instead of one shell, which is the energy conserving surface in momentum space for s-wave collisions, splitting in the Beliaev Damping spectrum would direct the colliding atoms into two separate shells [12]. Experimentally, the energy doublet can be observed by computerized tomography analysis of time of flight absorption images of the 3WM system [36].

In the presence of detuning, the Beliaev decay rate is calculated in a similar manner, again using Eq. (36). A damping spectrum for  $\Delta = \bar{\Omega}$  is shown as a dashed line in Fig. 16. The distance between the peaks increases with the detuning to a value of  $\Omega_{eff} \approx \sqrt{\bar{\Omega}^2 + \Delta^2}$ . As the detuning is increased, one peak grows while the other shrinks. For a positive (negative) detuning, the negative (positive) frequency peak becomes larger, whereas the magnitude of the positive (negative) energy peak decreases, for a large detuning, as  $1/\Delta^2$ . The perturbative result (thin dashed line) still fits the numerical prediction (thick dashed line) well. Deviations of the perturbative result are due to the non-linearity in  $m_x$  of the

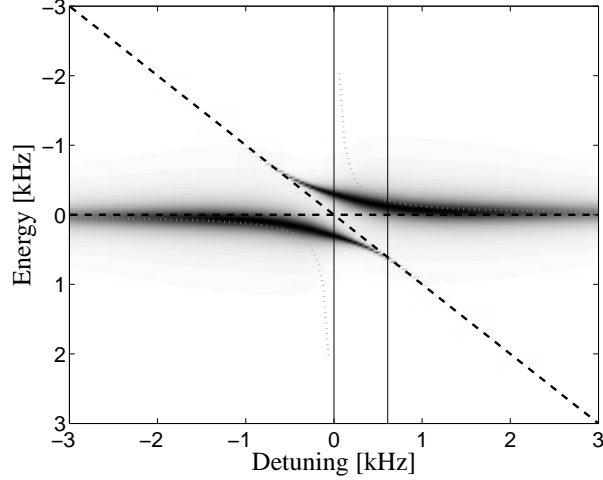


FIG. 17: The decay spectrum for different values of detuning. Darker areas correspond to higher transition rates. For large positive and negative detuning, the spectra asymptotically approach  $E = 0$  and  $E = \hbar\Delta$  (black dashed lines). The gray dotted line is the perturbative result of Eq. (14). The thin vertical lines are at the location of the spectra in Fig. 16.

transition probabilities between three-wave dressed states, while our model assumes these probabilities are linear as implied by Eq. (37).

In Fig. 17 we plot the spectrum vs. the detuning, where energy and detuning are in units of  $\hbar\bar{\Omega}$ . Darker areas in the graph correspond to higher transition rates. For a positive (negative) detuning, the center of the positive (negative) energy peak is approximately at  $E = \hbar\Delta$  (diagonal dashed line in Fig. 17). The center frequency of the negative (positive) frequency peak approaches  $E = 0$  (horizontal dashed line in Fig. 17) like  $1/\Delta$ . For a detuning larger than  $\bar{\Omega}$ , the center of the line is well approximated by the perturbative result given in Eq. (14).

Several additional mechanisms will contribute to the broadening of the two peaks beyond what is plotted in Fig. 16. The fact that only the first scattering event occurs between the  $N = M = 5 \times 10^3$  and the  $N = 5 \times 10^3 - 1$ ,  $M = 5 \times 10^3$  subspaces will broaden the resonances. Since the energy splitting scales as  $\sqrt{N}$ , in an experiment where one scatters  $dN$  atoms from mode  $\mathbf{k}$ , this will result in a relative broadening of  $dN/2N$ . According to the same scaling, an initial coherent, rather than Fock, state will cause a relative broadening of  $\sqrt{N}/2N$ . In the laboratory, the finite size and the inhomogeneous density profile of the trapped condensate, will cause additional broadening, and often dominate the width of the

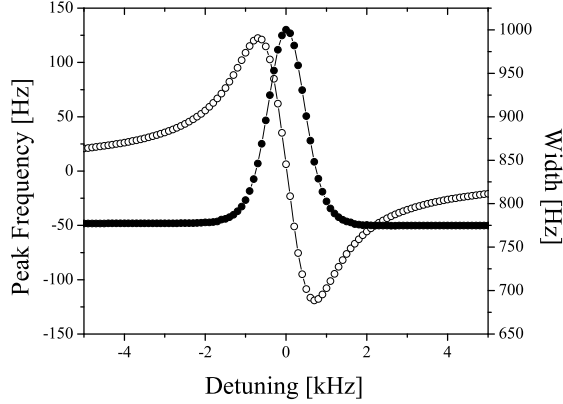


FIG. 18: The width (filled circles) and the peak location (empty circles) of the spectrum plotted in Fig. 17, in the presence of additional broadening taken to be a gaussian of width  $\bar{\Omega}$ . Although the broadening washed out the splitting, the broadening and resonance shift are still apparent.

Beliaev damping spectrum. In this case the doublet structure of the resonance may be unresolved, however the changes in the transition energies and heights, are translated to changes in the resonant frequency and the width of the collisional signal as shown in Fig. 18. There will be a broadening of the decay spectrum around  $\Delta = 0$ , whereas the energy of the collisional products will fall on a dispersive curve around the resonant value. Figure 18 indicates that even though splitting and oscillations may be difficult to observe when other decoherence mechanisms dominate over the 3WM coupling, line shifts and broadening can be still easily observed under such conditions.

Another way to measure this spectrum is by probing mode  $\mathbf{k}$  with a weak Bragg pulse. A spectrum obtained by setting the momentum of two laser beams, and sweeping the detuning between the beams, around the resonance of a quasiparticle excitation of the macroscopically occupied mode  $\mathbf{k}$ , is similar to that plotted in Fig. 16. When the wave mixing is resonant, there is a splitting in the spectrum, and when the wave mixing is non-resonant, one peak dominates, and in effect the spectrum is shifted as in the optical ac-Stark shift. We calculated the Bragg spectrum for the case where the momentum mode  $\mathbf{q}$  is probed rather than  $\mathbf{k}$ , and found that the spectrum would be a triplet rather than a doublet. This is in analogy to the Mollow splitting in atomic physics [16, 37].

In many experiments, the Beliaev damping is the main cause of decoherence. From Eq.



(35) it is clear that the total damping rate decreases for small values of  $k$ . This is due to a large reduction in the term  $A_{\mathbf{k},\mathbf{q}'}$ , and the smaller number of available modes into which decay is possible  $\mathbf{q}'$ . This suggests matter wave mixing experiments should be done in the low momentum three-wave regime rather than the high momentum four-wave regime.

In this section we focused on the Beliaev damping of three-wave mixing. The same arguments give rise to a splitting in the energy of Beliaev damping from a rapidly oscillating BEC discussed in sections II B, and III. We studied the Beliaev damping of such a system experimentally, and found a large deviation from the expected s-wave sphere [38].

## VI. CONCLUSION

In conclusion, we use the well known Schwinger boson mapping to describe the spectrum and dynamics of wave mixing. Motivated by matter wave mixing of Bose-Einstein condensates, we develop a framework for describing two and three-wave mixing. We first present the solution of a noninteracting two-wave mixing problem, corresponding to Rabi oscillations between two discrete momentum modes, induced by two-photon Bragg coupling. Interactions between modes are then added and the exact solution, obtained by diagonalizing the Hamiltonian is compared to a perturbative expansion. When the Rabi oscillation frequency  $\Omega$  is smaller than the chemical potential of the condensate  $\mu$ , the interactions are well described as a perturbation over the non-interacting solution, yielding a simple analytic expression for the non-linear quantum dephasing time. This dephasing is due to quantum fluctuations and cannot be described by mean field. The spectrum of such an oscillating BEC, can be calculated using this framework, and is found to agree with the measured one [22]. For a larger chemical potential, the perturbative solution breaks down, and differs from the exact solution. For  $\hbar\Omega = \mu$  the GPE is dynamically unstable, and cannot be used to predict dynamics. This case of two-mode dynamical instability is different than that of [39], which is an instability of a single Bloch state, and is under current experimental investigation.

We then analyze the spectrum and dynamics of three-wave mixing of Bogoliubov quasiparticles over a BEC. We study the spectrum and dynamics by treating the three-wave mixing locally as a two-wave mixing problem, multiplied by a factor representing the third field. By comparison to direct diagonalization of the three-wave mixing Hamiltonian, we

find this approximation to be valid even for small seeds  $M < N$ . We derive analytic expressions for the spectrum and decay time of the wave mixing oscillations at different detunings from the energy-conservation condition. We consider the coupling to the empty modes, and describe the damping from an oscillating mode due to collisions with the BEC. We use the local similarity to two-wave mixing to explain the underlying cause for the splitting in the spectrum of the Beliaev damping products obtained numerically from the exact three-wave diagonalization.

The Beliaev Damping phenomena studied in this paper, appear also in two-wave mixing. A Bose-Einstein condensate undergoing rapid Rabi oscillations, as presented in section II B, exhibits splitting in the Bragg spectrum of the different momentum modes, and in the Beliaev damping as well. Both these phenomena have been recently observed experimentally [22].

This dressed state approach can be extended to four-wave mixing of momentum modes  $\mathbf{k}_1, \mathbf{k}_2, \mathbf{k}_3$  and  $\mathbf{k}_4$ , where  $\mathbf{k}_1 + \mathbf{k}_2 = \mathbf{k}_3 + \mathbf{k}_4$  [1]. Here the conserved quantities are  $N = n_1 + n_2 + n_3 + n_4$ ,  $n_1 - n_2$ , and  $n_3 - n_4$ . If initially two modes are macroscopically occupied (say 1 and 3), the four-wave mixing is again similar to two-wave mixing of modes 2 and 4. Hence, one observes oscillatory dynamics which lead to a splitting in the decay spectrum.

Another case of three-wave mixing of bosonic matter waves is binary molecule formation. The Hamiltonian governing this process has been studied analytically for the case where both atoms are in the condensate mode [40]. Our model corresponds precisely to molecules formed of two separate atomic modes, and can be used to describe the evolution of such a system.

This work was supported in part by the Israel Ministry of Science, the Israel Science Foundation and by Minerva foundation.

- 
- [1] L. Deng, E. Hagley, J. Wen, M. Trippenbach, Y. Band, P. Julienne, J. Simsarian, K. Helmer-son, S. Rolston, and W. Phillips, *Nature (London)* **398**, 218 (1999).
  - [2] J. M. Vogels, J. K. Chin, and W. Ketterle, *Phys. Rev. Lett.* **90**, 030403 (2003).
  - [3] J. M. Vogels, K. Xu, and W. Ketterle, *Phys. Rev. Lett.* **89**, 020401 (2002).
  - [4] C. K. Hong and L. Mandel, *Phys. Rev. A* **31**, 2409 (1985).
  - [5] P. Bouyer and M. A. Kasevich, *Phys. Rev. A* **56**, R1083 (1997).

- [6] S. A. Morgan, S. Choi, K. Burnett, and M. Edwards, Phys. Rev. A **57**, 3818 (1998).
- [7] M. Trippenbach, Y. B. Band, and P. S. Julienne, Phys. Rev. A **62**, 023608 (2000).
- [8] E. V. Goldstein and P. Meystre, Phys. Rev. A **59**, 3896 (1999).
- [9] S. Inouye, T. Pfau, S. Gupta, A. P. Chikkatur, A. Görlitz, D. E. Pritchard, and W. Ketterle, Nature (London) **402**, 641 (1999).
- [10] S. Inouye, A. P. Chikkatur, D. M. Stamper-Kurn, J. Stenger, D. E. Pritchard, and W. Ketterle, Science **285**, 571 (1999).
- [11] D. Schneble, Y. Torii, M. Boyd, E. W. Streed, D. E. Pritchard, and W. Ketterle, Science **300**, 475 (2003).
- [12] R. Ozeri, N. Katz, J. Steinhauer, E. Rowen, and N. Davidson, Phys. Rev. Lett. **90**, 170401 (2003).
- [13] S. T. Beliaev, Sov. Phys. JETP **34(7)**, 299 (1958).
- [14] E. Hodby, O. M. Maragò, G. Hechenblaikner, and C. J. Foot, Phys. Rev. Lett. **86**, 2196 (2001).
- [15] N. Katz, J. Steinhauer, R. Ozeri, and N. Davidson, Phys. Rev. Lett. **89**, 220401 (2002).
- [16] C. Cohen-Tannoudji, J. Dupont-Roc, and G. Grynberg, *Atom-Photon interactions* (John Wiley & Sons Inc., 1992).
- [17] W. Ketterle and S. Inouye, C. R. Acad. Sci. Paris, Série IV **2**, 339 (2001).
- [18] J. R. Anglin and A. Vardi, Phys. Rev. A **64**, 013605 (2001).
- [19] N. Katz, R. Ozeri, E. Rowen, E. Gershnabel, and N. Davidson, Phys. Rev. A **70**, 033615 (2004).
- [20] A. L. Fetter, in *Proceedings of the international school of physics "Enrico Fermi", Course CXL*, edited by M. Inguscio, S. Stringari, and C. E. Wieman (IOS press, 1998), pp. 201–263.
- [21] P. B. Blakie and R. J. Ballagh, J. Phys. B **33**, 3961 (2000).
- [22] E. Rowen, N. Katz, R. Ozeri, E. Gershnabel, and N. Davidson (2004), cond-mat/0402225.
- [23] J. Hecker Denschlag, J. E. Simsarian, H. Häffner, C. McKenzie, A. Browaeys, D. Cho, K. Helmerson, S. L. Rolston, and W. D. Phillips, J. Phys. B **35**, 3095 (2002).
- [24] M. Tavis and F. W. Cummings, Phys. Rev. **170**, 379 (1968).
- [25] J. Schwinger, in *Quantum theory of angular momentum*, edited by L. C. Biedenharn and H. Van-Dam (Academic press, 1965), p. 229.
- [26] J. J. Sakurai, *Modern Quantum Mechanics* (Addison-Wesely Publishing company, 1994), re.

ed.

- [27] E. P. Wigner, *Group Theory and its application to the quantum mechanics of atomic spectra*, vol. 5 of *Pure and Applied Physics* (Academic Press, New-York, 1959).
- [28] D. J. Rowe, H. de Guise, and B. C. Sanders, J. Math. Phys. **42**, 2315 (2001).
- [29] T. Tyc and B. C. Sanders, J. Phys. A **37**, 7341 (2004), quant-ph/0404090.
- [30] F. Zambelli, L. Pitaevskii, D. M. Stamper-Kurn, and S. Stringari, Phys. Rev. A **61**, 063608 (2000).
- [31] A. Smerzi, S. Fantoni, S. Giovanazzi, and S. R. Shenoy, Phys. Rev. Lett. **79**, 4950 (1997).
- [32] S. L. Cornish, N. R. Claussen, J. L. Roberts, E. A. Cornell, and C. E. Wieman, Phys. Rev. Lett. **85**, 1795 (2000).
- [33] J. Steinhauer, R. Ozeri, N. Katz, and N. Davidson, Phys. Rev. Lett. **88**, 120407 (2002).
- [34] S. H. Autler and C. H. Townes, Phys. Rev. **100**, 703 (1955).
- [35] D. Tannor, *Introduction to Quantum Mechanics: A Time-dependent Perspective* (University Science Books, Sausalito, 2005).
- [36] R. Ozeri, J. Steinhauer, N. Katz, and N. Davidson, Phys. Rev. Lett. **88**, 220401 (2002).
- [37] B. R. Mollow, in *Progress in Optics*, edited by E. Wolf (North-Holland, Amsterdam, 1981), vol. XIX.
- [38] N. Katz, E. Rowen, R. Ozeri, and N. Davidson (2005), submitted to Phys. Rev. Lett., cond-mat/0505762.
- [39] L. Fallani, L. De Sarlo, J. E. Lye, M. Modugno, R. Saers, C. Fort, and M. Inguscio, Phys. Rev. Lett. **93**, 140406 (2004).
- [40] A. Vardi, V. A. Yurovsky, and J. R. Anglin, Phys. Rev. A **64**, 063611 (2001).